RNA-binding protein network alteration causes aberrant axon branching and growth phenotypes in FUS ALS mutant motoneurons

Maria Giovanna Garone[1], Nicol Birsa[2,3], Maria Rosito[4], Federico Salaris[1,4], Michela Mochi[1], Valeria de Turris[4], Remya R. Nair[5], Thomas J. Cunningham[5], Elizabeth M. C. Fisher[2], Pietro Fratta[2] and Alessandro Rosa[1,4,6,*]

1. Department of Biology and Biotechnology Charles Darwin, Sapienza University of Rome, P.le A. Moro 5, 00185 Rome, Italy
2. UCL Queen Square Institute of Neurology, University College London, London, WC1N 3BG, UK
3. UK Dementia Research Institute, University College London, London, WC1E 6BT, UK
4. Center for Life Nano Science, Istituto Italiano di Tecnologia, Viale Regina Elena 291, 00161 Rome, Italy
5. MRC Harwell Institute, Oxfordshire, OX11 0RD, UK
6. Laboratory Affiliated to Istituto Pasteur Italia-Fondazione Cenci Bolognetti, Department of Biology and Biotechnology Charles Darwin, Sapienza University of Rome, Viale Regina Elena 291, 00161 Rome, Italy

* Corresponding author: alessandro.rosa@uniroma1.it; Tel: +39-0649255218

ABSTRACT

Mutations in RNA-binding proteins (RBPs) have been genetically associated with the motoneuron disease Amyotrophic Lateral Sclerosis (ALS). Using both human induced Pluripotent Stem Cells and mouse models, we found that FUS-ALS causative mutations have a profound impact on a network of RBPs, including two relevant factors with important roles in neuronal RNA metabolism: HuD and FMRP. Mechanistically, cytoplasmic localization of mutant FUS leads to upregulation of HuD levels through competition with FMRP for HuD 3'UTR binding. In turn, increased HuD levels overly stabilize the transcript levels of its targets, NRN1 and GAP43. As a consequence, mutant FUS motoneurons show altered axon branching and growth upon injury. Abnormal axon branching and regrowth in FUS mutant motoneurons could be rescued by dampening NRN1 levels. Since similar phenotypes have been previously described in SOD1 and TDP-43 mutant models, aberrant axonal growth and branching might represent broad early events in the pathogenesis of ALS.

Keywords

Amyotrophic Lateral Sclerosis; FUS; HuD; ELAVL4; FMR1; FMRP; NRN1; GAP43; iPSC; motoneuron; axon; 3'UTR.

INTRODUCTION

The motoneuron disease Amyotrophic Lateral Sclerosis (ALS) has been linked to mutations in several RNA binding proteins (RBPs), including the most frequently occurring ones in the TARDBP (TDP-43) and FUS genes, and altered RNA metabolism [1]. Despite a recent increase in our knowledge of the genetics of ALS, the disease mechanisms downstream of mutations in ALS-genes remain largely uncharacterized. The most severe ALS mutations in the RBP FUS lie within its C-terminal nuclear localization signal (PY-NLS domain), impairing the interaction with the nuclear import receptor Transportin-1 (TNPO1) and reducing nuclear localization [2]. Loss of FUS and TDP-43 nuclear functions, including regulation of alternative splicing and polyadenylation, has been proposed as a pathological mechanism [3-5]. Insoluble cytoplasmatic aggregates containing ALS-linked RBPs are a hallmark of the pathology [6], and gain of toxic cytoplasmic functions may also play important roles in ALS [7].

We previously observed strong correlation between changes in protein levels and selective binding of mutant FUS to 3′UTR [8], suggesting that aberrant targeting of 3′UTRs by mutant FUS likely represents a broad mechanism underlying proteome alteration in motoneurons (MNs). This is particularly relevant for ALS-linked genes, genes encoding for cytoskeletal proteins and, notably, other RBPs [8,9]. Importantly, cellular levels of ALS-linked RBPs are tightly regulated by both auto-regulation mechanisms [10-12] and cross-regulatory mechanisms [9,12-16]. The neural RBP HuD (encoded by the *ELAVL4* gene), a novel component of cytoplasmic inclusions in FUS, TDP-43 and sporadic ALS patients [9,14], represents an example of such cross-regulation. We have found aberrantly increased HuD levels in *FUS* mutant MNs due to microRNA-mediated effects, and direct binding of mutant FUS to the *HuD* 3'UTR, by a still uncharacterized mechanism [9,17]. HuD is a neural translation enhancer and its overexpression induces increased neurite outgrowth in neuronal cell lines and primary neural progenitor cells [18-20], but whether the alteration of HuD levels has functional consequences in *FUS* mutant MNs remains unexplored.

Axonal degeneration is a key feature in the ALS pathophysiology and occurs prior to the motor phenotype in patients [21-23]. The levels of cytoskeletal proteins and factors directing neuron projection are changed in *FUS* mutant hiPSC-derived MNs [8], and aberrant branching and axonal outgrowth have been recently identified across ALS mutations and model systems, underlying their importance in early disease pathogenesis [24-28]. Spinal MNs isolated from adult *SOD1* mutant mice at pre-symptomatic stages displayed significant increase in axon outgrowth, in terms of length and branching complexity, and acute expression of mutant SOD1 in WT MNs was sufficient to increase axonal regeneration [29]. These evidences point to axonal alteration as an early, pre-symptomatic phenotype in ALS.

Here we provide a mechanistic link between aberrant axonal phenotypes and alteration of a cross-regulatory circuitry involving three RBPs: FUS, HuD and the fragile X mental retardation protein (FMRP). We find that FMRP is a novel negative regulator of *HuD* translation via 3'UTR binding. We propose that this function is outcompeted by mutant FUS binding to the same regulatory region, leading to an increase in HuD protein level, thus providing a mechanistic explanation of HuD upregulation in *FUS* mutant MNs. Further, we identify altered axonal growth as a functional consequence of HuD upregulation, and finally find it to be mediated by the alteration of the HuD target NRN1.

RESULTS

ALS mutant FUS competes with FMRP for *HuD* regulation via 3'UTR binding

We have previously found mutant FUS to lead to an increase in HuD [9,17]. Although miR-375 may play a role [17,30], experiments conducted in the absence of miR-375 indicate that a further regulation mechanism is also present. Interestingly, *HuD* 3'UTR is extensively conserved in vertebrates, with a high phyloP100way score (mean: 4.8; standard deviation: 2.3), approaching that

of coding exons (e.g. exon 2, mean: 5.9; standard deviation: 3.2) and not restricted to miR-375 binding sites (Supplementary Figure S1), further supporting the existence of another regulatory mechanism.

In order to gain insights into HuD regulation in ALS, we took advantage of spinal MNs derived from isogenic pairs of FUS WT and P525L hiPSC lines (hereafter FUS^{WT} and FUS^{P525L}) [31,32]. In parallel, we used the Fus-Δ14 knock-in mouse model, in which a frameshift mutation leads to a complete loss of the nuclear localization signal (NLS) [33]. In both human *in vitro* MNs (Figure 1A) and mouse spinal cords (post-natal day 81, P81) (Figure 1B), we observed a two-fold increase of HuD protein levels in *FUS* mutant genetic backgrounds. Fluorescence in situ hybridization (FISH) analysis showed a significant increase in the number of HuD puncta in FUS^{P525L} human MNs (Figure 1C). We next took advantage of puro-PLA, a technique that couples puromycylation with the proximity-ligation assay to visualize newly synthesized proteins [34]. Puro-PLA was performed on FUS^{P525L} and FUS^{WT} human MNs using and anti-HuD antibody, revealing an increase in newly synthetised HuD in mutant cells (Figure 1D; Supplementary Figure S2). Increased HuD translation was also detected in primary MNs from the Fus-Δ14 mouse model (Figure 1E).

Together with our previous work [9], these observations suggest that mutant FUS might trigger HuD translation upregulation via 3'UTR binding. Mechanistically, this effect could arise from the competition with an inhibitory RBP. We used *cat*RAPID [35] to predict the interactors of the HuD 3'UTR. Several RBPs showed interaction propensity with this sequence (Supplementary Table S1), and we filtered this list for ones involved in the regulation of translation (GO:0006412) (Supplementary Table S2). Among these candidates, we focused on negative regulators of translation and noticed FMRP, encoded by the fragile X mental retardation 1 (FMR1) gene. Native RNA immunoprecipitation (RIP) was used to validate the physical association between FMRP and the *HuD* transcript. FMRP was effectively immunoprecipitated from hiPSC-derived MN extracts

(Figure 2A). A hemizygous FMRP knock-out human iPSC line ($FMRP^{KO}$), generated by CRISPR/Cas9-mediated modification of a male line (hereafter $FMRP^{WT}$) (Supplementary Figure S3), served as a negative control. Quantitative RT-PCR analysis revealed specific enrichment of the *MAP1B* mRNA, a well-characterized FMRP interactor [36,37], and no enrichment of a negative control, the housekeeping *ATP5O* mRNA, in the FMRP immunoprecipitated samples (Figure 2B). Consistent with the *cat*RAPID prediction, FMRP immunoprecipitation enriched the *HuD* mRNA (Figure 2B). Both *MAP1B* and *HuD* were negligible in the immunoprecipitated samples from the control $FMRP^{KO}$ line, confirming the RIP specificity (Supplementary Figure S3D). In MNs obtained from $FMRP^{KO}$ iPSCs, HuD protein levels were increased of approximately two-fold (Figure 2C). In the same cells, HuD transcript levels were unchanged (Figure 2D), suggesting that absence of FMRP upregulated HuD protein without altering its transcription or mRNA stability. Notably, *HuD* mRNA levels were reduced in FMRP immunoprecipitated samples from FUS^{P525L} MNs (Figure 2B). Consistent with a previous report [14], we also observed reduced interaction between FMRP and *MAP1B* mRNA in FUS mutant cells (Figure 2B). Decreased interaction with its targets was not consequence of lower FMRP protein level in FUS^{P525L} MNs (Supplementary Figure S3E).

We then took advantage of a reporter assay to study the outcomes of possible competitive binding of FMRP and mutant FUS to the *HuD* 3'UTR. We have previously described that expression of FUS^{P525L} led to increased translation of a luciferase construct carrying the *HuD* 3'UTR [9]. In the same experimental setup, overexpression of FMRP reversed this effect (Figure 2E).

Collectively, these results suggest that FMRP can act as negative regulator of HuD translation in MNs by direct 3'UTR binding. Mutant FUS may intrude in this function, possibly by competition for 3'UTR binding, resulting in increased HuD protein levels.

Axon branching and growth phenotypes in FUS mutant MNs

Since HuD protein levels are two- to four-fold higher in human and mouse *FUS* mutant MNs compared to wild-type controls (Figure 1A-B), we wondered if such upregulation could lead to

functional consequences. Overexpression of HuD promotes neurite outgrowth in rat PC12 cells (a cell line of neural crest origin) and cortical neurons [18,19], and we therefore took advantage of multichambered microfluidics devices to study possible neurodevelopmental defects in *FUS* mutant MNs. FUS^{WT} and FUS^{P525L} human MN progenitors were dissociated and re-plated into one chamber (cell body chamber) of compartmentalized chips with 500 μm microgroove barrier. Such experimental setup allowed us to analyze axons in a separate compartment (axon chamber). Axonal morphology was analyzed after subsequent MN maturation in the device for 7 days. As shown in Figure 3A, we found an increased number of axon branches and junctions in the FUS mutant compared to WT. A similar increase in axon branching was recently reported by Akiyama and colleagues in MNs derived from human iPSCs carrying a different FUS mutation (H517D) [28]. We further extended this analysis by evaluating axon regeneration after damage. At the sixth day of maturation, chemical axotomy was induced by applying trypsin to the axonal chamber. MNs were then allowed to regenerate their axons for 30 hours. Immunostaining of the neuronal tubulin TUBB3 showed strikingly increased outgrowth in FUS^{P525L} cells (Figure 3C; Supplementary Figure S4). Similar results were obtained when axotomy was induced in the same experimental setup by vacuum application (mechanical injury) or digestion with a different chemical agent, accutase (Figure 3D-E). These results were independently confirmed in the Fus-Δ14 mouse model. Primary embryonic MNs, derived from heterozygous and homozygous mutant mice (E12.5-13.5) and plated in compartmentalized chips, showed increased arborization when compared to WT controls (Figure 4A,B). Increased re-growth was also observed for axotomized *Fus* mutant mouse MNs (Figure 4C).

Altered NRN1 and GAP43 levels in FUS mutant motoneurons

We next focused on downstream HuD targets, which could be altered as a consequence of increased levels of this RBP in FUS mutant MNs, and that might be involved in the aberrant axon phenotypes observed in these cells. Among other known HuD targets we prioritized *NRN1* and *GAP43*.

HuD stabilizes the mRNA encoding the neurotrophic factor NRN1 (Neuritin1) by binding its 3'UTR [38], and we found *NRN1* mRNA levels to be strongly increased in FUS^{P525L} MNs as assessed by quantitative RT-PCR (Figure 5A) and FISH analyses (Figure 5B). Western blot analysis showed that NRN1 protein levels are negligible in FUS^{WT} MNs and increased in FUS^{P525L} cells (Figure 5C). This observation was confirmed in the mouse model, where P81 spinal cord samples showed increased levels of the mouse Nrn1 homolog in heterozygous and homozygous mutants (Figure 5D). Immunostaining analysis in human MNs showed that NRN1 is expressed at low levels in the WT axons and is upregulated in the FUS mutant axons (Figure 5E). Previous work showed that HuD overexpression increased *GAP43* mRNA levels in rat cortical neurons [19]. In particular, HuD binds to an AU-rich regulatory element (ARE) in the 3′UTR of *GAP43* mRNA and stabilizes this transcript [39,40]. As in the case of *NRN1*, increased levels of *GAP43* mRNA were observed in FUS^{P525L} MNs by quantitative RT-PCR and FISH (Figure 5A and Figure 6A). An increase of GAP43 protein levels in the FUS mutant background was detected by western blot analysis in hiPSC-derived MNs but not in mouse spinal cord (Figure 6B,C). The increase in GAP43 protein levels in FUS^{P525L} human MNs was confirmed by immunostaining analysis (Figure 6D). Increase of *HuD*, *NRN1* and *GAP43* mRNA and protein levels was confirmed in MNs generated from two additional FUS^{P525L} human iPSC lines [41] (Supplementary Figures S5 and S6).

To directly correlate NRN1 and GAP43 upregulation to increased HuD activity, we generated a HuD overexpressing hiPSC line in a FUS^{WT} background. Overexpression of HuD in undifferentiated iPSCs by a constitutive promoter resulted in cell toxicity. We therefore took advantage of a neuronal-specific human synapsin 1 promoter construct (SYN1::HuD) to drive expression of HuD after induction of MN differentiation (Supplementary Figure S7A). Rise of HuD in FUS^{WT} SYN1::HuD MNs was in the range of HuD levels observed in FUS^{P525L} MNs (FUS^{WT}+HuD in Figure 1C and 5A and in Supplementary Figure S7B-E). In these cells, we observed increased levels of *NRN1* and *GAP43* mRNA (Figure 5A). In the case of *GAP43*,

however, change in mRNA levels between FUS^{WT} and FUS^{WT}+HuD did not reach statistical significance. Finally, increased transcript and protein levels of *NRN1* and, to a lesser extent, *GAP43* were detected in $FMRP^{KO}$ MNs, where HuD protein levels were upregulated (Figure 2C,D). Collectively these data point to increased levels of HuD targets in FUS mutant MNs as a consequence of the disruption of the FMRP-mediated negative regulation of HuD by FUS^{P525L}. In particular, NRN1 is strongly upregulated, while GAP43 is affected in the same direction, although to a minor extent.

Aberrant axonal phenotypes of mutant motoneurons are due to NRN1 upregulation

Given the greater changes in NRN1 levels, compared to GAP43, in FUS mutant MNs, we decided to prioritize this candidate for further analysis. Upon activation by neural activity and neurotrophins, NRN1 plays a positive role in promoting neurite outgrowth and arborization [42-46]. Increased levels of NRN1 in FUS mutant MNs prompted us to explore the possibility that the phenotypes described in Figures 3 and 4 are a direct consequence of aberrant activation of this neurotrophic factor. We addressed this hypothesis by a rescue approach. Small interfering RNAs (siRNAs), transfected during hiPSC-derived MN maturation, effectively reduced NRN1 levels in the FUS^{P525L} background (Figure 7A). In siRNA-NRN1-treated FUS^{P525L} MNs cultured in microfluidics devices we observed reduced number of axon branches and junctions, compared to non-targeting control siRNAs (Figure 7B). We next performed in these cells the trypsin-induced axotomy and regeneration assay as in Figure 3D. TUBB3 immunostaining analysis showed that axon growth after regeneration was strongly reduced in FUS^{P525L} MNs treated with NRN1-siRNAs (Figure 7C). These results suggest that aberrant axon branching and growth observed in FUS mutant MNs are mediated by increased levels of NRN1 and that knock-down of NRN1 is sufficient to revert these phenotypes.

DISCUSSION

Here we propose a novel regulatory mechanism for *HuD* translation in normal MNs and its alteration in ALS. A relevant consequence of HuD upregulation in FUS mutant MNs is the increase of two HuD targets: NRN1 and GAP43. In turn, NRN1 hyperactivation confers aberrant axon branching and growth upon axotomy to FUS mutant MNs.

According to our model (Figure 8), a mutation that impairs the nuclear localization of FUS may trigger a domino effect onto other RBPs. One of the consequences is the escape of *HuD* from negative regulation by FMRP on its 3'UTR. The highly conserved *HuD* 3'UTR is indeed a relevant regulatory element, with an important role in keeping HuD protein levels in check. For this purpose, we propose that at least two distinct mechanisms are in place in MNs. The first one involves the activity of the MN-enriched microRNA, miR-375 [17]. The second one, described in this work, relies on the negative regulation of translation by FMRP. Notably, both mechanisms are impaired by FUS mutations. We indeed previously observed reduced levels of miR-375 in FUS mutant MNs [17]. Interestingly, impaired miR-375 function has been also proposed by others in a mouse model of sporadic ALS [47] and in another MN disease, type1 SMA [48].

ALS FUS mutations would also impair FMRP-mediated repression of *HuD*. This might occur in several, non-exclusive, possible ways. First, FMRP might be captured in mutant FUS insoluble aggregates, as proposed by Blokhuis and colleagues [14], who also reported impaired FMRP-mediated translational repression and altered MAP1B protein levels in cells overexpressing mutant FUS. In both FUS^{P525L} hiPSC-derived MNs and Fus-Δ14 mice, however, mutant FUS is expressed at physiological levels and does not form aggregates [9,33,49]. Second, FUS mutations might promote phase separation of FMRP by sequestering it in FUS-containing cytoplasmic ribonucleoprotein complexes (RNPs) (Birsa et al., *in preparation*). Third, mutant FUS might directly compete with FMRP for 3'UTR binding. HuD 3'UTR contains multiple putative regulatory elements and competitive or cooperative 3'UTR binding is a regulatory mechanism extensively

used by RBPs [50,51]. Interestingly, loss of the FMRP homolog dFXR leads to NMJ defects in Drosophila [52], while exogenous FMRP expression rescued NMJ and locomotor defects in a zebrafish FUS ALS model [14]. Recent evidence has also linked FMRP with TDP-43 [53,54], suggesting that FMRP involvement in ALS might extend beyond FUS.

Increased HuD suggested a possible underlying mechanism for the aberrant axon branching and growth phenotypes that we observed in both human and mouse ALS FUS models. HuD has indeed a well-known role in promoting neurogenesis in cell lines and cortical neurons [18,19]. However, to our knowledge, the role of HuD in MNs has never been specifically addressed. Here we show that at least two relevant HuD targets are upregulated in FUS mutant MNs as a consequence of loss of HuD repression: GAP43 and NRN1. GAP43 is upregulated downstream of increased HuD during axon regeneration upon sciatic nerve injury [55]. In a transgenic mouse model, overexpression of GAP43 induces prolonged nerve sprouting and causes death of adult MNs [56,57]. Together with our present findings, those observations suggest that GAP43 aberrant increase might in part contribute to the pathogenic effects of FUS mutations in ALS MNs.

The neurotrophic factor NRN1 is one of the primary HuD targets in MNs. HuD stabilizes NRN1 mRNA via AU-rich element binding on its 3'UTR [38,58]. NRN1, also known as CPG15, was first identified as a candidate plasticity-related gene (CPG) induced by the glutamate analogue kainate in the hippocampus dentate gyrus, along with immediate early genes (IEGs) such as c-Fos and c-Jun [42]. It was later demonstrated that NRN1 is an activity-regulated IEG induced by calcium influx through NMDA receptors and L-type voltage-sensitive calcium channels [59]. Its expression in the rat neocortex peaks at 14 days postnatal and then decreases in the adult [60]. In the adult rat, NRN1 mRNA is detected in brain regions characterized for their activity-modulated plasticity (hippocampus, olfactory bulb and Purkinje cells) and can be induced by glutamate analogs, neurotrophins (such as BDNF) and neural activity [43]. In the Human Protein Atlas [61], the spinal

cord is reported among the nervous system regions with lowest NRN1 expression (Supplementary Figure S8). We found increased NRN1 levels in FUS mutant hiPSC-derived MNs and mouse spinal cord, in the absence of promoting stimuli. NRN1 was also upregulated upon HuD overexpression and FMRP knock-out. When overexpressed in rodent or Xenopus neurons, NRN1 induced neurite outgrowth, elaboration of dendritic and axonal arbors and synaptic maturation by AMPA receptor insertion [43-45]. NRN1 is highly expressed in developing MNs, where its overexpression increases axonal outgrowth and neurite branching [62]. This effect is remarkably similar to aberrant phenotypes observed in motor neurons expressing the ALS SOD1-G93A mutant [29]. Consistently, increased axon branching and growth upon axotomy occurring in our mutant FUS models could be rescued by reduction of NRN1 levels with siRNAs. This result suggests that increased NRN1 mRNA stability, downstream of HuD upregulation, may be one of the key aberrant mechanisms underlying the observed axon phenotypes.

Consistent with our findings, Akiyama and colleagues have recently reported an aberrant axon branching phenotype in iPSC-derived MNs carrying the FUS^{H517D} mutation [28]. They also showed increased levels of AP-1 components (including members of the FOS family) and reversion of the axon branching phenotype upon FOS-B reduction [28]. AP-1 increase might not directly contribute to NRN1 upregulation in FUS mutant cells. In stimulated cortical neurons, indeed, NRN1 upregulation occurred independently from new protein synthesis, indicating that NRN1 induction does not require prior activation of AP-1 [59]. Therefore, the effects observed by Akiyama and colleagues upon modulation of FOS-B are unlikely mediated by NRN1. To the best of our knowledge, NRN1 has been never associated with ALS before. However, by mining published RNA-Seq datasets we found an upregulation trend of the *Nrn1*/*NRN1* transcript in the soma of MNs dissected from a SOD1 mouse model at a pre-symptomatic stage (3 months) [63] or generated from SOD1 mutant human and mouse stem cells [64]. Pro-regenerative effects on adult MNs upon ALS-mutant SOD1 expression have been recently shown, including increased outgrowth and branching

[29]. This is unlikely a compensatory response to mutant SOD1-induced toxicity, as it occurs also upon acute expression of mutant SOD1 in WT adult MNs. Notably, MN axon branching was also increased in zebrafish embryos injected with ALS-mutant TDP-43 proteins, which showed a motor deficit [26]. The importance of aberrant axon branching and growth in ALS pathophysiology deserves more investigation, as it might be detrimental for the normal function of signal transmission in MNs [24]. Our work provides new insights into the molecular mechanisms underlying such axonal phenotypes in FUS-ALS.

MATERIALS AND METHODS

Plasmids construction

The epB-Puro-TT-SYN1-HuD (SYN1::HuD) and epB-Puro-TT-SYN1-RFP (SYN1::RFP) plasmids were generated by inserting the sequences of the human synapsin 1 (SYN1) promoter and, respectively, Flag-HA-HuD and tagRFP in the enhanced piggyBac transposable vector epB-Puro-TT [65]. The SYN1 promoter was isolated from the eMSCL WT plasmid (Addgene, #107454) via PCR with the following primers: hSYN1 FW 5'-CATCTCGAGCAGTGCAAGTGGGTTTTAGGAC-3'; hSYN1 RV 5'-CATGGATCCACTGCGCTCTCAGGCACGA-3'. Flag-HA-HuD was obtained by cutting the pFRT-TODestFLAGHA_HuD plasmid (Addgene, #65757) with PaeI and BglII enzymes. The resulting constructs contain the enhanced piggyBac terminal repeats flanking a constitutive cassette driving the expression of the puromycin resistance gene fused to the rtTA gene and, in the opposite direction, a SYN1 promoter driving the expression of the transgenes (Supplementary Figure S7). ePB-Bsd-TT-FMR1. The epB-NIL vector for spinal MN differentiation, containing the Ngn2, Isl1 and Lhx3 transgenes, is described in [31].

iPSC culture, differentiation and transfection

Generation of the iPSC lines WT I and FUS-P525L/P525L is described in [49]. KOLF iPSCs WT 2 and P525L16 (LL FUS-eGFP) and T12.9 iPSCs WT15 and P525L17 (SL FUS-eGFP) are a kind gift of J. Sterneckert [41]. The FMR1 KO hiPSC line was generated by CRISPR/Cas9 gene editing from the WT I line, as described in Supplementary Figure S3. Maintenance conditions of iPSCs are described in [49]. iPSCs were co-transfected with 4.5 μg of transposable vector (epB-NIL, SYN1::HuD, SYN1::RFP) and 0.5 μg of the piggyBac transposase using the Neon Transfection System (Life Technologies), as described [49]. Selection was carried out in 5 μg/ml blasticidin S (for epB-NIL) and 1 μg/ml puromycin (for SYN1::HuD, SYN1::RFP), giving rise to stable cell lines.

The spinal MN differentiation protocol is detailed in [31,32]. Briefly, epB-NIL-containing cells were differentiated upon induction with 1 μg/ml doxycycline (Thermo Fisher Scientific) in DMEM/F12 (Sigma-Aldrich), supplemented with 1X Glutamax (Thermo Fisher Scientific), 1X NEAA (Thermo Fisher Scientific) and 0.5X Penicillin/Streptomycin (Sigma-Aldrich) for 2 days and Neurobasal/B27 medium (Neurobasal Medium, Thermo Fisher Scientific; supplemented with 1X B27, Thermo Fisher Scientific; 1X Glutamax, Thermo Fisher Scientific; 1X NEAA, Thermo Fisher Scientific; and 0.5X Penicillin/Streptomycin, Sigma Aldrich), containing 5 μM DAPT and 4 μM SU5402 (both from Sigma-Aldrich) for additional 3 days. At day 5, MN progenitors were dissociated with Accutase (Thermo Fisher Scientific) and plated on Matrigel (BD Biosciences)-coated 15 mm diameter dishes or cover glass (0.13-0.17 thick), or bipartite/tripartite microfluidic chambers (MFCs, see below) at the density of 10^5 cells per cm^2. 10 μM rock inhibitor was added for the first 24 hours after dissociation. Neuronal cultures were maintained in neuronal medium (Neurobasal/ B27 medium supplemented with 20 ng/ml BDNF and 10 ng/ml GDNF, both from PreproTech; and 20 ng/ml L-ascorbic acid, Sigma-Aldrich). MFCs were made with Sylgard 184 silicone elastomer kit (Dow Corning) using epoxy resin molds. Once the MFCs were baked, reservoirs were cut and the MFCs were mounted onto glass-bottom dishes (HBST-5040, WillCo well), pre-coated with 1:200 100X poly-D-Lysine. MFCs were then blocked with 0.8% BSA in ES

(Sigma-Aldrich) overnight and then coated with Matrigel (BD Biosciences), before plating MN progenitors. MFCs have 500 μm long grooves that separate the somatic from the axonal compartment.

Mouse primary motoneurons

Fus-Δ14 mice (B6N;B6J-Fus$^{tm1Emcf/H}$, MGI: 6100933) were previously described [33]. All applicable international, national, and institutional guidelines, including ARRIVE guidelines, for the care and use of animals were followed. All procedures performed in studies involving animals were in accordance with the ethical standards of the institution at which the studies were conducted (University College London, UK; MRC Harwell Institute, Oxfordshire, UK). All procedures for the care and treatment of animals were in accordance with the Animals (Scientific Procedures) Act 1986 Amendment Regulations 2012. Primary MNs (PMNs) were isolated from E12.5-13.5 mouse embryos on a congenic C57BL/6J background. Briefly, embryos were euthanized, spinal cord removed and ventral regions isolated. PMNs were dissociated by incubation with trypsin, followed by mechanical dissociation in combination with DNase treatment. Cells were then centrifuged through a bovine serum albumin (BSA) cushion and resuspended in motor neuron medium (Neurobasal; Thermo Fisher, Waltham, MA), 2% v/v B27 supplement (Thermo Fisher Scientific), 2% heat-inactivated horse serum (HRS), 1X GlutaMAX (Thermo Fisher Scientific), 24.8 μM β-mercaptoethanol, 10 ng/ml rat ciliary neurotrophic factor (CNTF; R&D Systems), 0.1 ng/ml rat glial cell line-derived neurotrophic factor (GDNF; R&D systems), 1 ng/ml human brain-derived neurotrophic factor (BDNF; PeproTech) and 1% penicillin/streptomycin. PMNs were immediately plated on poly-L-ornithine/laminin- coated plates or MFCs and cultured for 6-7 days at 37°C in a 5% CO_2 incubator.

Adult spinal cord samples were collected from female Fus-Δ14 mice on a (C57BL/6J x DBA/2J) F1 hybrid background, via laminectomy, and snap frozen over liquid nitrogen. The hybrid background

was necessary to produce viable homozygotes, which are non-viable on a congenic C57BL/6J background.

Western blot

Western blot analysis was carried out using anti-HuD (1:1000; sc-48421, Santa Cruz), anti-NEURITIN (1:200; AF283, R&D Systems), anti-GAP43 (1:500; LS-C356053, Bio-techne), anti-TUBB3 (1:10000; T2200, Sigma-Aldrich), anti-GAPDH (1:2000; MAB-10578 Immunological sciences) primary antibodies and donkey anti-mouse IgG (H+L) (IS20404; Immunological Science) and donkey anti-rabbit IgG (H+L) (IS20405; Immunological Science) secondary antibodies, as previously described [9].

Real-time qRT-PCR

Total RNA, extracted with the RNA extract kit ($1x10^6$ cells-10mg; VWR International PBI) and retrotranscribed with iScript Supermix (Bio-Rad Laboratories), was analyzed by real-time qRT-PCR with iTaq Universal SYBR Green Supermix (Bio-Rad Laboratories). *ATP5O* was used as the internal calibrator. Primers sequences are listed in Supplementary Table S3.

RNA interference (RNAi)

NRN1 RNAi was induced with a synthetic siRNA pool targeting the human NRN1 mRNA (NRN1 51299 siRNA-SMARTpool, Dharmacon) or with a non-targeting siRNA control pool with scrambled sequence (ON-TARGETplus Non-targeting Pool; D-001810-10-05, Dharmacon). Lyophilized siRNAs were resuspended in nuclease-free water and stored at –20 °C as 20 μM stocks until use. For transfection, siRNAs were diluted in Optimem (Gibco) and mixed with siLentFect Lipid Reagent (Bio-Rad Laboratories), according to the protocol for transfection of adherent cells. The final siRNA concentration in each MFC was 10 nM. Medium was changed 5 hours post-transfection.

Immunofluorescence

Cells were fixed in 4% paraformaldehyde (PFA) in PBS for 10 min at room temperature. Coverslips were washed with PBS, permeabilized and blocked for 15 min using a solution of 0.5% BSA, 10% HRS, 0.2% Triton X-100 in PBS (all from Sigma-Aldrich). Anti-TUJ1 (for TUBB3 detection; 1:1000; T2200, Sigma-Aldrich), anti-GAP-43 (1:500; LS-C356053, Bio-techne), anti-MAP2 (1:2000; ab5392, Abcam), anti-NEURITIN (1:200; AF283, R&D Systems) antibodies were diluted in a solution of 0.5% BSA, 10% HRS in PBS and incubated with the cells for 1 hr at room temperature. Cells were then washed in PBS and incubated for 1 hr at room temperature with the appropriate fluorescent conjugated secondary anti-mouse Alexa Fluor 488 (1:200, Thermo Fisher Scientific), anti-rabbit Alexa Fluor 594 (1:200, Immunological Sciences) and anti-goat Alexa Fluor 594 (1:200, Immunological Sciences) donkey secondary antibodies and DAPI (1:2,000; Sigma-Aldrich) diluted in 0.5% BSA, 10% HRS in PBS. Finally, cells were washed with PBS, mounted using DAKO mounting media and imaged using inverted Zeiss LSM 780 or 510 confocal microscopes using a 63×, 1.4 NA DIC Plan-Apochromat oil-immersion objective, except for images shown in Figure 7C, which have been acquired with an inverted Olympus iX73 equipped with an X-Light V3 spinning disc head (Crest Optics), a LDI laser illuminator using 470 nm wavelength (89 North), a CoolSNAP MYO CCD camera (Photometrics) and MetaMorph software (Molecular Devices) with a 10× objective.

Puro-PLA

Cells were treated with either DMSO or 40 μM anisomycin for 30 min. Then, 2 μM puromycin was added to the medium for 7 min at 37°C in a 5% CO_2 incubator, cells were washed 2 times with PBS and fixed in 4% PFA in PBS for 12 min at room temperature. Coverslips were permeabilized with 0.2% Triton X-100 in PBS for 15 min and blocked using a solution of 0.5% BSA and 10% HRS in PBS for 30 min. Detection of newly synthesized proteins was carried out by an anti-puromycin

antibody (clone 12D10, mouse-monoclonal, MABE343; Merck), an anti-HuD antibody (ab96474, rabbit-monoclonal; Abcam) and Duolink PLA Fluorescence reagents Red (DUO92008, Duolink), according to manufacturer's instructions, using rabbit PLAplus (DUO92002, Duolink) and mouse PLAminus (DUO92004, Duolink). The anti-TUJ1 antibody was used as a cell marker and to identify axons, as described in the 'Immunofluorescence' section. All samples were mounted in Duolink In Situ Mounting Media with DAPI (DUO82040, Duolink).

Fluorescence in situ hybridization (FISH)

Cells were fixed for 15 min with 4% PFA in PBS. FISH was performed with the QuantiGene ViewRNA ISH Cell Assay (Thermo Fisher Scientific) protocol for adherent cells. Briefly, fixed MNs were rinsed 3 times in PBS containing 5 mM $MgCl_2$ for 5 min. Cells were then dehydrated in ethanol (50%,75%,100%) for 2 min each and stored at -20°C for up to one week, minimum of 2 hours. Coverslips were rehydrated (75%, 50%) for 2 min each and washed 3 times in PBS containing 5 mM $MgCl_2$ for 5 min. Coverslips were permeabilized with Detergent Solution and then treated with Protease QS (1:8000). FISH was carried out following manufacturer's instructions (QVC000; Thermo Fisher Scientific). Cells were mounted using DAKO mounting media or Prolong Gold with DAPI (Invitrogen) and imaged using an inverted Zeiss LSM 780 or 510 confocal microscope using a 63X, 1.4 NA DIC Plan-Apochromat oil-immersion objective and Zeiss LSM 880 laser scanning confocal microscope.

RNA immunoprecipitation (RIP)

iPSC-derived motor neurons at day 12 of differentiation were lysed with PLB Buffer (5 mM $MgCl_2$, 10 mM HEPES (pH 7.0), 150 mM KCl, 5 mM EDTA (pH 8), 0.5% NP-40, 2 mM DTT, with 100 U/ml RNAase inhibitor and 1X protease inhibitor cocktail), incubated for 5 minutes on ice and centrifuged 10 minutes at 4°C at 14000g. Protein concentration of the supernatant was then measured by Bradford assay and a volume containing 1 mg of proteins was diluted in NT2 Buffer

(50 mM Tris (pH 7), 150 mM NaCl, 0.5 mM $MgCl_2$, 0.05% NP-40, 1 mM DTT, 20 mM EDTA (pH 8) with 100 U/ml RNAse inhibitor and 1X protease inhibitor cocktail). Protein G-coupled dynabeads (immunoprecipitation kit, Invitrogen) were washed in NT2 Buffer, incubated with 10 µg of anti-FMRP (f4055, Sigma Aldrich) or rabbit monoclonal anti-human IgG antibody (ab109489, Abcam) and left rotating on a wheel for 1 hour at room temperature in NT2 Buffer. Beads were then washed in NT2 Buffer and incubated with the diluted lysates in a final volume of 500 µl. Binding was carried out at 4°C with the samples rotating on a wheel for 2 hours. Beads were then washed 3 times and resuspended in ice-cold NT2. Each sample was split 1/5 for protein and 4/5 for RNA analysis. The protein fraction was resuspended in 1X NuPage LDS (Invitrogen) with 2 mM DTT and left at 70°C for 20 minutes. Proteins were run on a 4%–12% polyacrylamide gel for 1 hour at 160 V. The RNA fraction was lysed with 250 µl of TRIzol (Invitrogen) and extracted according to manufacturer's instructions. RNA was analyzed by real-time qRT-PCR with iTaq Universal SYBR Green Supermix (Bio-Rad Laboratories). RIP data analysis was performed as follows. For each target, the mean Ct value from a technical duplicate was normalized to the input RNA fraction (at a 1/10 dilution) Ct value (ΔCt) to account for RNA sample preparation differences, using the equation: $\Delta Ct = [Ct_{RIP\ or\ IgG} - Ct_{input} - Log_2 10]$. The percentage of input was calculated by linear conversion of the normalized ΔCt as $2^{-\Delta Ct}$. This value was then adjusted to take into account the difference in the amplification of the artificial spike RNA between the control IgG and the IP fractions.

Luciferase assay

The pSI-Check2 vector containing HuD 3'UTR (RLuc-HuD 3'UTR) is described in [9]. RLuc-HuD 3'UTR was transfected alone or in combination with epB-Bsd-TT-FMR1 or epB-Bsd-TT-eGFP in $5x10^4$ pre-seeded HeLa cells expressing RFP-FUS^{P525L} [9] in a 24-well plate using Lipofectamine 2000 (Life Technologies), following manufacturer's instructions. Cells were harvested 24 hours

post-transfection and RLuc and FLuc activities were measured by Dual Glo luciferase assay (Promega), according to the manufacturer's protocol.

Axon branching and growth upon axotomy assays

After dissociation at day 5 of differentiation, hiPSC-derived MNs were grown in microfluidics for 7 days. Axotomy was then performed using 3 different methods: 1) Trypsin-EDTA 0.25% (Thermo Fisher Scientific) treatment for 15 min (Figure 3C, 4C, 7C; Supplementary Figure 4); 2) repeated vacuum aspirations (Figure 3D); 3) Accutase (Thermo Fisher Scientific) treatment for 15 min (Figure 3E). The axon chamber was reperfused with PBS until effective removal of the damaged axons, without disturbing the cell bodies in the soma compartment.

Quantitative analyses of axon branches and junctions were conducted with Skeleton, a plugin of Fiji [66]. 30 hours after axotomy, immunofluorescence staining with an anti-TUJ1 antibody was performed as described in the 'Immunofluorescence' section.

Data availability

All data generated or analyzed during this study are included in this published article and its supplementary information files.

COMPETING INTERESTS

The authors declare that they have no competing interests.

FUNDING

This work was partially supported by Sapienza University, Fondazione Istituto Italiano di Tecnologia and a grant from Istituto Pasteur Italia - Fondazione Cenci Bolognetti to A.R. P.F., T.J.C., R.R.N. and E.M.C.F., were funded by grants from the UK Medical Research Council.

AUTHORS' CONTRIBUTIONS

Conceptualization, M.G.G. and A.R.; Formal analysis, M.G.G., N.B., M.R.; Investigation, M.G.G., N.B., F.S.; Methodology, M.G.G., F.S., M.M., V.d.T., R.R.N.; Project administration, A.R.; Supervision, A.R., P.F., E.M.C.F. and T.J.C.; Writing – original draft, A.R.

All authors read and approved the final manuscript.

ACKNOWLEDGMENTS

The authors wish to thank the Imaging Facility at Center for Life Nano Science, Istituto Italiano di Tecnologia, for support and technical advice. We are grateful to Jared Sterneckert (Technische Universität Dresden, Germany) for sharing their human iPSC lines. We thank Riccardo De Santis (The Rockefeller University, NY, USA), Serena Carra (University of Modena and Reggio Emilia, Italy) and Silvia Di Angelantonio and Irene Bozzoni (Sapienza University of Rome, Italy) for helpful discussion.

REFERENCES

1. Brown, R. H. & Al-Chalabi, A. Amyotrophic Lateral Sclerosis. *N Engl J Med* **377,** 162–172 (2017).

2. Dormann, D. *et al*. ALS-associated fused in sarcoma (FUS) mutations disrupt Transportin-mediated nuclear import. *EMBO J* **29,** 2841–2857 (2010).

3. Lagier-Tourenne, C. *et al*. Divergent roles of ALS-linked proteins FUS/TLS and TDP-43 intersect in processing long pre-mRNAs. *Nat Neurosci* (2012). doi:10.1038/nn.3230

4. Klim, J. R. *et al*. ALS-implicated protein TDP-43 sustains levels of STMN2, a mediator of motor neuron growth and repair. *Nat Neurosci* **22,** 167–179 (2019).

5. Melamed, Z. *et al*. Premature polyadenylation-mediated loss of stathmin-2 is a hallmark of TDP-43-dependent neurodegeneration. *Nat Neurosci* **22,** 180–190 (2019).

6. Dormann, D. & Haass, C. TDP-43 and FUS: a nuclear affair. *Trends in neurosciences* **34,** 339–348 (2011).

7. Birsa, N., Bentham, M. P. & Fratta, P. Cytoplasmic functions of TDP-43 and FUS and their role in ALS. *Semin Cell Dev Biol* (2019). doi:10.1016/j.semcdb.2019.05.023

8. Garone, M. G. *et al*. Proteomics analysis of FUS mutant human motoneurons reveals altered regulation of cytoskeleton and other ALS-linked proteins via 3'UTR binding. *Sci Rep* **10,** 11827 (2020).

9. De Santis, R. *et al*. Mutant FUS and ELAVL4 (HuD) Aberrant Crosstalk in Amyotrophic Lateral Sclerosis. *Cell Rep* **27,** 3818–3831.e5 (2019).

10. Ayala, Y. M. *et al*. TDP-43 regulates its mRNA levels through a negative feedback loop. *EMBO J* **30,** 277–288 (2011).

11. Zhou, Y., Liu, S., Liu, G., Oztürk, A. & Hicks, G. G. ALS-associated FUS mutations result in compromised FUS alternative splicing and autoregulation. *PLoS Genet* **9,** e1003895 (2013).

12. Humphrey, J. *et al*. FUS ALS-causative mutations impair FUS autoregulation and splicing factor networks through intron retention. *Nucleic Acids Res* (2020). doi:10.1093/nar/gkaa410

13. Huelga, S. C. *et al*. Integrative genome-wide analysis reveals cooperative regulation of alternative splicing by hnRNP proteins. *Cell Rep* **1,** 167–178 (2012).

14. Blokhuis, A. M. *et al*. Comparative interactomics analysis of different ALS-associated proteins identifies converging molecular pathways. *Acta Neuropathol* **132,** 175–196 (2016).

15. Mohagheghi, F. *et al*. TDP-43 functions within a network of hnRNP proteins to inhibit the production of a truncated human SORT1 receptor. *Hum Mol Genet* **25,** 534–545 (2016).

16. Gueroussov, S. *et al*. Regulatory Expansion in Mammals of Multivalent hnRNP Assemblies that Globally Control Alternative Splicing. *Cell* **170,** 324–339.e23 (2017).

17. De Santis, R. *et al*. FUS Mutant Human Motoneurons Display Altered Transcriptome and microRNA Pathways with Implications for ALS Pathogenesis. *Stem Cell Reports* **9,** 1450–1462 (2017).

18. Anderson, K. D. *et al*. Overexpression of HuD, but not of its truncated form HuD I+II, promotes GAP-43 gene expression and neurite outgrowth in PC12 cells in the absence of nerve growth factor. *Journal of neurochemistry* **75,** 1103–1114 (2000).

19. Anderson, K. D. *et al*. Overexpression of HuD accelerates neurite outgrowth and increases GAP-43 mRNA expression in cortical neurons and retinoic acid-induced embryonic stem cells in vitro. *Exp Neurol* **168,** 250–258 (2001).

20. Tebaldi, T. *et al*. HuD Is a Neural Translation Enhancer Acting on mTORC1-Responsive Genes and Counteracted by the Y3 Small Non-coding RNA. *Mol Cell* **71,** 256–270.e10 (2018).

21. Fischer, L. R. *et al*. Amyotrophic lateral sclerosis is a distal axonopathy: evidence in mice and man. *Exp Neurol* **185,** 232–240 (2004).

22. Roy, S., Zhang, B., Lee, V. M.-Y. & Trojanowski, J. Q. Axonal transport defects: a common theme in neurodegenerative diseases. *Acta Neuropathol* **109,** 5–13 (2005).

23. Ferraiuolo, L., Kirby, J., Grierson, A. J., Sendtner, M. & Shaw, P. J. Molecular pathways of motor neuron injury in amyotrophic lateral sclerosis. *Nat Rev Neurol* **7,** 616–630 (2011).

24. Suzuki, N., Akiyama, T., Warita, H. & Aoki, M. Omics Approach to Axonal Dysfunction of Motor Neurons in Amyotrophic Lateral Sclerosis (ALS). *Front Neurosci* **14,** 194 (2020).

25. McWhorter, M. L., Monani, U. R., Burghes, A. H. M. & Beattie, C. E. Knockdown of the survival motor neuron (Smn) protein in zebrafish causes defects in motor axon outgrowth and pathfinding. *J Cell Biol* **162,** 919–931 (2003).

26. Kabashi, E. *et al*. Gain and loss of function of ALS-related mutations of TARDBP (TDP-43) cause motor deficits in vivo. *Hum Mol Genet* **19,** 671–683 (2010).

27. Hogan, A. L. *et al*. Expression of ALS/FTD-linked mutant CCNF in zebrafish leads to increased cell death in the spinal cord and an aberrant motor phenotype. *Hum Mol Genet* **26,** 2616–2626 (2017).

28. Akiyama, T. *et al*. Aberrant axon branching via Fos-B dysregulation in FUS-ALS motor neurons. *EBioMedicine* **45,** 362–378 (2019).

29. Osking, Z. *et al*. ALS-Linked SOD1 Mutants Enhance Neurite Outgrowth and Branching in Adult Motor Neurons. *iScience* **11,** 294–304 (2019).

30. Abdelmohsen, K. *et al*. miR-375 inhibits differentiation of neurites by lowering HuD levels. *Mol Cell Biol* **30,** 4197–4210 (2010).

31. De Santis, R. *et al*. Direct conversion of human pluripotent stem cells into cranial motor neurons using a piggyBac vector. *Stem Cell Research* **29,** 189–196 (2018).

32. Garone, M. G. *et al*. Conversion of Human Induced Pluripotent Stem Cells (iPSCs) into Functional Spinal and Cranial Motor Neurons Using PiggyBac Vectors. *J Vis Exp* (2019). doi:10.3791/59321

33. Devoy, A. *et al*. Humanized mutant FUS drives progressive motor neuron degeneration without aggregation in 'FUSDelta14' knockin mice. *Brain* **140,** 2797–2805 (2017).

34. tom Dieck, S. *et al*. Direct visualization of newly synthesized target proteins in situ. *Nat Methods* **12,** 411–414 (2015).

35. Agostini, F. *et al*. catRAPID omics: a web server for large-scale prediction of protein-RNA interactions. *Bioinformatics* **29,** 2928–2930 (2013).

36. Brown, V. *et al*. Microarray identification of FMRP-associated brain mRNAs and altered mRNA translational profiles in fragile X syndrome. *Cell* **107**, 477–487 (2001).

37. Darnell, J. C. *et al*. Fragile X mental retardation protein targets G quartet mRNAs important for neuronal function. *Cell* **107,** 489–499 (2001).

38. Akten, B. *et al*. Interaction of survival of motor neuron (SMN) and HuD proteins with mRNA cpg15 rescues motor neuron axonal deficits. *Proc Natl Acad Sci USA* **108,** 10337–10342 (2011).

39. Mobarak, C. D. *et al*. The RNA-binding protein HuD is required for GAP-43 mRNA stability, GAP-43 gene expression, and PKC-dependent neurite outgrowth in PC12 cells. *Mol Biol Cell* **11,** 3191–3203 (2000).

40. Beckel-Mitchener, A. C., Miera, A., Keller, R. & Perrone-Bizzozero, N. I. Poly(A) tail length-dependent stabilization of GAP-43 mRNA by the RNA-binding protein HuD. *J Biol Chem* **277,** 27996–28002 (2002).

41. Marrone, L. *et al*. Isogenic FUS-eGFP iPSC Reporter Lines Enable Quantification of FUS Stress Granule Pathology that Is Rescued by Drugs Inducing Autophagy. *Stem Cell Reports* **10,** 375–389 (2018).

42. Nedivi, E., Hevroni, D., Naot, D., Israeli, D. & Citri, Y. Numerous candidate plasticity-related genes revealed by differential cDNA cloning. *Nature* **363,** 718–722 (1993).

43. Naeve, G. S. *et al*. Neuritin: a gene induced by neural activity and neurotrophins that promotes neuritogenesis. *Proc Natl Acad Sci USA* **94,** 2648–2653 (1997).

44. Nedivi, E., Wu, G. Y. & Cline, H. T. Promotion of dendritic growth by CPG15, an activity-induced signaling molecule. *Science* **281,** 1863–1866 (1998).

45. Cantallops, I., Haas, K. & Cline, H. T. Postsynaptic CPG15 promotes synaptic maturation and presynaptic axon arbor elaboration in vivo. *Nat Neurosci* **3,** 1004–1011 (2000).

46. Zhao, Q.-R., Lu, J.-M., Li, Z.-Y. & Mei, Y.-A. Neuritin promotes neurite and spine growth in rat cerebellar granule cells via L-type calcium channel-mediated calcium influx. *Journal of neurochemistry* **147,** 40–57 (2018).

47. Rohm, M. *et al*. The microRNA miR-375-3p and the Tumor Suppressor NDRG2 are Involved in Sporadic Amyotrophic Lateral Sclerosis. *Cell. Physiol. Biochem*. **52,** 1412–1426 (2019).

48. Bhinge, A. *et al*. MiR-375 is Essential for Human Spinal Motor Neuron Development and May Be Involved in Motor Neuron Degeneration. *Stem Cells* **34,** 124–134 (2016).

49. Lenzi, J. *et al*. ALS mutant FUS proteins are recruited into stress granules in induced Pluripotent Stem Cells (iPSCs) derived motoneurons. *Dis Model Mech* **8,** 755–766 (2015).

50. Bronicki, L. M. & Jasmin, B. J. Emerging complexity of the HuD/ELAVl4 gene; implications for neuronal development, function, and dysfunction. *RNA* **19,** 1019–1037 (2013).

51. García-Mauriño, S. M. *et al*. RNA Binding Protein Regulation and Cross-Talk in the Control of AU-rich mRNA Fate. *Front Mol Biosci* **4,** 1271 (2017).

52. Zhang, Y. Q. *et al*. Drosophila fragile X-related gene regulates the MAP1B homolog Futsch to control synaptic structure and function. *Cell* **107,** 591–603 (2001).

53. Coyne, A. N. *et al*. Fragile X protein mitigates TDP-43 toxicity by remodeling RNA granules and restoring translation. *Hum Mol Genet* **24,** 6886–6898 (2015).

54. Majumder, P., Chu, J.-F., Chatterjee, B., Swamy, K. B. S. & Shen, C.-K. J. Co-regulation of mRNA translation by TDP-43 and Fragile X Syndrome protein FMRP. *Acta Neuropathol* **132,** 721–738 (2016).

55. Yoo, S. *et al*. A HuD-ZBP1 ribonucleoprotein complex localizes GAP-43 mRNA into axons through its 3' untranslated region AU-rich regulatory element. *Journal of neurochemistry* **126,** 792–804 (2013).

56. Aigner, L. *et al*. Overexpression of the neural growth-associated protein GAP-43 induces nerve sprouting in the adult nervous system of transgenic mice. *Cell* **83,** 269–278 (1995).

57. Harding, D. I., Greensmith, L., Mason, M., Anderson, P. N. & Vrbová, G. Overexpression of GAP-43 induces prolonged sprouting and causes death of adult motoneurons. *Eur J Neurosci* **11,** 2237–2242 (1999).

58. Wang, Z.-H. *et al*. HuD regulates the cpg15 expression via the 3'-UTR and AU-rich element. *Neurochem. Res*. **36,** 1027–1036 (2011).

59. Fujino, T., Lee, W.-C. A. & Nedivi, E. Regulation of cpg15 by signaling pathways that mediate synaptic plasticity. *Mol Cell Neurosci* **24,** 538–554 (2003).

60. Nedivi, E., Fieldust, S., Theill, L. E. & Hevron, D. A set of genes expressed in response to light in the adult cerebral cortex and regulated during development. *Proc Natl Acad Sci USA* **93,** 2048–2053 (1996).

61. Uhlén, M. *et al*. Proteomics. Tissue-based map of the human proteome. *Science* **347,** 1260419 (2015).

62. Javaherian, A. & Cline, H. T. Coordinated motor neuron axon growth and neuromuscular synaptogenesis are promoted by CPG15 in vivo. *Neuron* **45,** 505–512 (2005).

63. Bandyopadhyay, U. *et al*. RNA-Seq profiling of spinal cord motor neurons from a presymptomatic SOD1 ALS mouse. *PLoS ONE* **8,** e53575 (2013).

64. Nijssen, J., Aguila, J., Hoogstraaten, R., Kee, N. & Hedlund, E. Axon-Seq Decodes the Motor Axon Transcriptome and Its Modulation in Response to ALS. *Stem Cell Reports* **11,** 1565–1578 (2018).

65. Rosa, A., Papaioannou, M. D., Krzyspiak, J. E. & Brivanlou, A. H. miR-373 is regulated by TGFβ signaling and promotes mesendoderm differentiation in human Embryonic Stem Cells. *Dev Biol* (2014). doi:10.1016/j.ydbio.2014.03.020

66. Schindelin, J. *et al*. Fiji: an open-source platform for biological-image analysis. *Nat Methods* **9,** 676–682 (2012).

FIGURE LEGENDS

Figure 1. Increased HuD levels in human and mouse FUS-mutant MNs.

(A,B) HuD protein levels analysis by western blot in FUS^{WT} and FUS^{P525L} hiPSC-derived spinal MNs (A) and Fus-Δ14 mouse model spinal cord (P81) (B). The graphs show the average from 3 independent biological replicates, error bars indicate the standard deviation (panel A: Student's t-test, paired, two tails, *$p < 0.05$; panel B: ordinary one-way ANOVA, multiple comparisons, **$p < 0.01$, ns: $p > 0.05$). TUBB3/Tubb3 signal was used for normalization. (C) HuD mRNA analysis by FISH in FUS^{WT} and FUS^{P525L} hiPSC-derived spinal MNs. The graphs show the average count of HuD mRNA puncta per cell from 2 independent differentiation experiments, error bars indicate the standard deviation (Student's t-test; paired; two tails; ****$p < 0.0001$; ns: $p > 0.05$). (D,E) Combined PURO-PLA (HuD, magenta) and immunostaining (TUBB3, green) analysis in FUS^{WT} and FUS^{P525L} hiPSC-derived spinal MNs (D) and primary MNs from Fus-Δ14 mouse embryos (E12.5-13.5) (E). DAPI (blue) was used for nuclear staining. The graphs show the average count of HuD PURO-PLA mRNA puncta per cell from 3 independent differentiation experiments (D) and 2 samples (E), error bars indicate the standard deviation (panel D: Student's t-test, unpaired, two tails, ****$p < 0.0001$; panel E: ordinary one-way ANOVA, multiple comparisons, ****$p < 0.0001$, ns: $p > 0.05$). Scale bars in panels (C,D,E): 10 μm.

Figure 2. FMRP is a post-transcriptional repressor of HuD expression

(A) Western blot analysis of the FMRP RIP assay. In: input; IgG: control immunoprecipitation with rabbit monoclonal anti-human IgG antibody; IP: samples immunoprecipitated with an anti-FMRP antibody. (B) Analysis of *MAP1B* (positive control), *ATP5O* (negative control) and *HuD* mRNA levels by real time qRT-PCR in samples from FUS^{WT} (top) or FUS^{P525L} (bottom) hiPSC-derived spinal MNs. Values on the graphs are reported as the percentage of input in IP or control IgG samples, after normalization with an artificial spike RNA. The graphs show the average from 3 independent differentiation experiments and error bars indicate the standard deviation. (C) Analysis

of the protein levels of the indicated genes by western blot in $FMRP^{WT}$ and $FMRP^{KO}$ hiPSC-derived spinal MNs. The graphs show the average from 3 independent differentiation experiments, error bars indicate the standard deviation (Student's t-test; paired; two tails; *$p < 0.05$). TUBB3 signal was used for normalization. (D) Analysis of the mRNA levels of the indicated genes by real-time qRT-PCR in $FMRP^{WT}$ and $FMRP^{KO}$ hiPSC-derived spinal MNs. For each experiment, values are shown as relative to the isogenic $FMRP^{WT}$ control, set to a value of 1. The graph shows the average from 3-5 independent differentiation experiments, error bars indicate the standard deviation (Student's t-test; paired; two tails; p values are indicated; ns: $p > 0.05$). (E) Luciferase assay in HeLa cells expressing RFP-FUS^{P525L} and transfected with the Renilla luciferase reporter construct containing the HuD 3'UTR (RLuc-HuD 3'UTR) in combination with plasmids overexpressing FMRP or eGFP as a control (Student's t-test; paired; two tails; ***$p < 0.001$; ns: $p > 0.05$). The drawing on the right depicts the competition between mutant FUS and FMRP for HuD 3'UTR binding and its effects on the reporter construct.

Figure 3. Axonal phenotypes in hiPSC-derived spinal MNs

(A) Representative images, generated with the Skeleton plugin of ImageJ, showing axons of FUS^{WT} and FUS^{P525L} human iPSC-derived MNs in the axon chamber of compartmentalized chips. Scale bar: 100 μm. (B) Quantitative analysis of the number of axon branches and junctions in cells shown in (A). The graphs show the average from 3 independent differentiation experiments, error bars indicate the standard deviation (Student's t-test; unpaired; two tails; ****$p < 0.0001$). (C-E) Immunostaining of TUBB3 (green) in FUS^{WT} and FUS^{P525L} hiPSC-derived spinal MNs cultured in compartmentalized chips and allowed to recover for 30 hours after the indicated treatments to induce axotomy in the axon chamber. Scale bar: 50 μm

Figure 4. Axonal phenotypes in primary spinal MNs from Fus-Δ14 mouse models

(A) Representative images, generated with the Skeleton plugin of ImageJ, showing axons of $Fus^{+/+}$, and heterozygous ($Fus^{\Delta 14/+}$) or homozygous ($Fus^{\Delta 14/\Delta 14}$) FUS mutant mouse primary MNs in the axon chamber of compartmentalized chips. Scale bar: 100 µm. (B) Quantitative analysis of the number of axon branches and junctions in cells shown in (A). The graphs show the average from 3 biological replicates, error bars indicate the standard deviation (Ordinary one-way ANOVA; multiple comparisons; ****$p < 0.0001$). (C) Immunostaining of Tubb3 (green) in $Fus^{+/+}$, $Fus^{\Delta 14/+}$ and $Fus^{\Delta 14/\Delta 14}$ mouse primary MNs cultured in compartmentalized chips and allowed to recover for 30 hours after trypsin treatment to induce axotomy in the axon chamber. Scale bar: 100 µm.

Figure 5. NRN1 levels are increased in mutant FUS MNs

(A) Analysis of the mRNA levels of the indicated genes by real time qRT-PCR in FUS^{WT}, FUS^{P525L} and FUS^{WT} overexpressing HuD under the SYN1 promoter (FUS^{WT}+HuD) hiPSC-derived spinal MNs. The graph shows the average from 4 independent differentiation experiments, error bars indicate the standard deviation (Student's t-test; paired; two tails; *$p < 0.05$; **$p < 0.01$; ***$p < 0.001$; ns: $p > 0.05$). (B) NRN1 mRNA analysis by FISH (red) in FUS^{WT} and FUS^{P525L} hiPSC-derived spinal MNs. DAPI (blue) was used for nuclear staining. Scale bar: 10 µm. Graphs show the average count of HuD mRNA puncta per cell and the puncta intensity from 3 independent differentiation experiments, error bars indicate the standard deviation (Student's t-test; unpaired; two tails; ****$p < 0.0001$). (C,D) NRN1 protein levels analysis by western blot in FUS^{WT} and FUS^{P525L} hiPSC-derived spinal MNs (C) and Fus-Δ14 mouse model spinal cord (D). The graphs show the average from 3 independent biological replicates, error bars indicate the standard deviation (Ordinary one-way ANOVA; multiple comparisons; *$p < 0.05$). (E) Immunostaining analysis of NRN1 in axons of FUS^{WT} and FUS^{P525L} hiPSC-derived spinal MNs. The graph shows the NRN1 signal intensity from 2 independent differentiation experiments, error bars indicate the standard deviation (Student's t-test; unpaired; two tails; ****$p < 0.0001$).

Figure 6. GAP-43 levels are increased in mutant FUS MNs

(A) GAP-43 mRNA analysis by FISH (red) in FUS^{WT}, FUS^{P525L} and FUS^{WT} overexpressing HuD under the Syn1 promoter (FUS^{WT}+HuD) hiPSC-derived spinal MNs. The graphs show the average count of HuD mRNA puncta per cell from 3 independent differentiation experiments, error bars indicate the standard deviation (Student's t-test; unpaired; two tails; ****$p < 0.0001$). DAPI (blue) was used for nuclear staining. Scale bar: 10 μm. (B) GAP43 protein levels analysis by western blot in FUS^{WT} and FUS^{P525L} hiPSC-derived spinal MNs. The graph shows the average from 3 independent differentiation experiments and error bars indicate the standard deviation (Student's t-test; paired; two tails; *$p < 0.05$). TUBB3 signal was used for normalization. (C) Gap43 protein level analysis by western blot in mouse primary spinal MNs (P81). The graphs show the average from 3 mice and error bars indicate the standard deviation. The differences are not significant for all pairs (ordinary one-way ANOVA; multiple comparisons). Tubb3 signal was used for normalization. (D) Immunostaining analysis in FUS^{WT}, FUS^{P525L} and FUS^{WT} overexpressing HuD under the SYN1 promoter (FUS^{WT}+HuD) hiPSC-derived spinal MNs. GAP-43 signal is magenta; MAP2 signal is green. DAPI (blue) was used for nuclear staining. The graph shows the NRN1 signal intensity from 3 independent differentiation experiments, error bars indicate the standard deviation (Student's t test; unpaired; two tails; ****$p < 0.0001$). Scale bar: 10 μm.

Figure 7. NRN1 knockdown rescues the aberrant axon growth phenotype in mutant FUS MNs

(A) Analysis of the mRNA levels of the indicated genes by real time qRT-PCR in untransfected FUS^{WT} and FUS^{P525L} hiPSC-derived spinal MNs and FUS^{P525L} hiPSC-derived spinal MNs transfected with non-targeting control siRNAs or siRNAs targeting NRN1. The graph shows the average of a technical triplicate, error bars indicate the standard deviation. (B) Quantitative analysis of the number of axon branches and junctions. Immunostaining of TUBB3 was carried out 5 days after transfection of the indicated siRNA pools in FUS^{P525L} human iPSC-derived MNs cultured in compartmentalized chips. The graphs show the average from 2 independent differentiation

experiments, error bars indicate the standard deviation (Student's t-test; unpaired; two tails; ****$p < 0.0001$). (C) Immunostaining of TUBB3 (green) in FUS^{P525L} hiPSC-derived spinal MNs cultured in compartmentalized chips, transfected with non-targeting control siRNAs or siRNAs targeting NRN1, treated with trypsin in the axon chamber to induce axotomy after 24 hours, and allowed to recover for 24 hours. DAPI (blue) was used for nuclear staining. Scale bar: 100 μm.

Figure 8. Model

The figure depicts a model of the competition between mutant FUS and FMRP for HuD 3'UTR binding. In FUS^{WT} MNs (top), the FUS protein is predominantly localized in the nucleus. In the cytoplasm, FMRP binds HuD 3'UTR repressing its translation. NRN1 mRNAs are destabilized. In FUS^{P525L} MNs, mutant FUS is partially delocalized to the cytoplasm and outcompetes FMRP binding on the HuD 3'UTR. As a consequence, increased HuD protein levels accumulate in FUS mutant MNs. HuD binding to NRN1 and GAP-43 3'UTR leads to stabilization of these transcripts and higher protein levels. NRN1 increase underlies the aberrant axonal growth phenotypes.

A

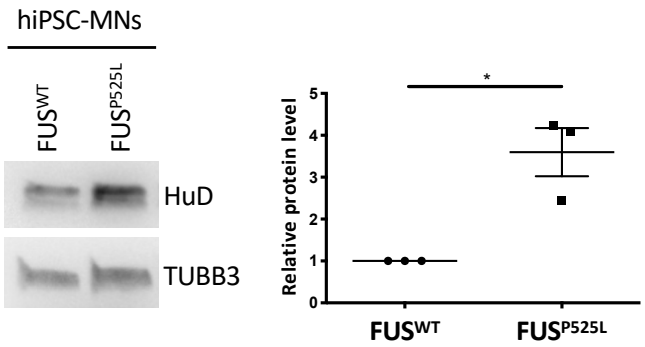

B

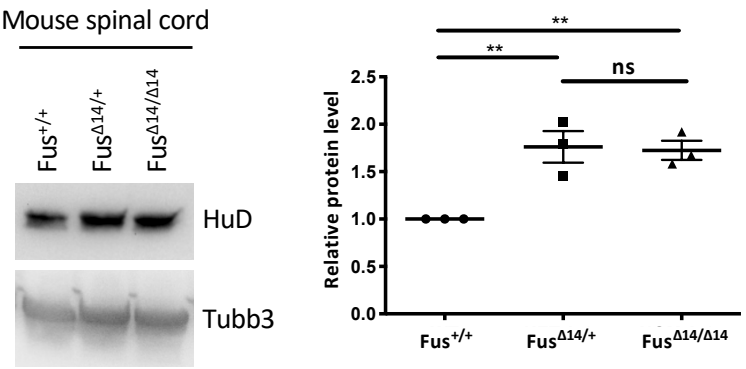

C

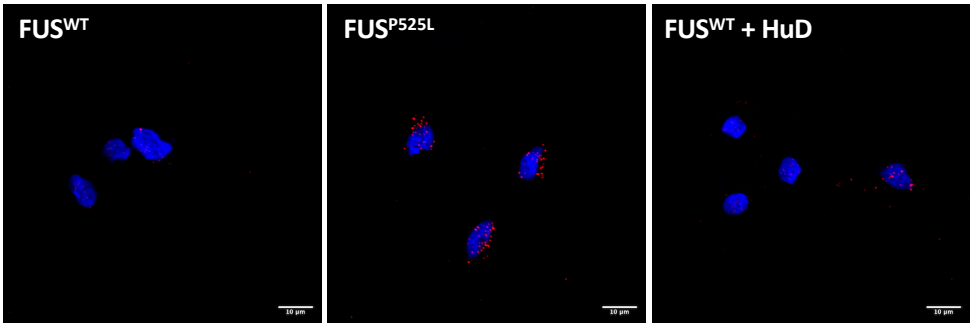

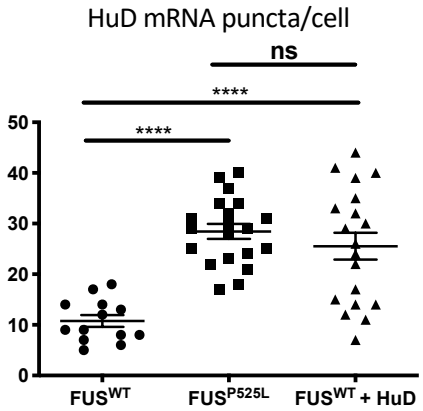

D

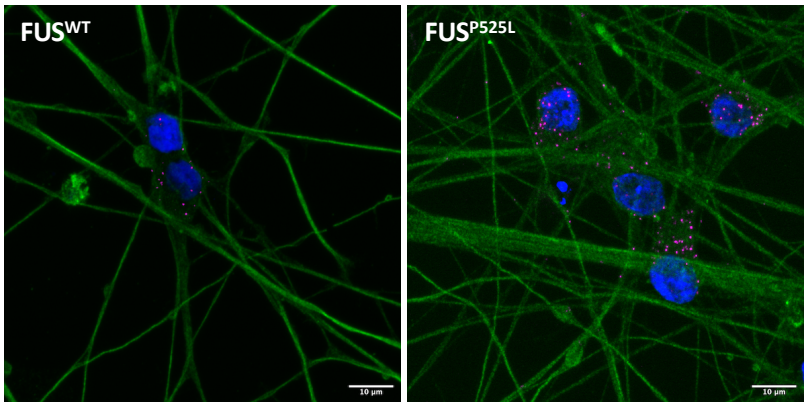

DAPI HuD PURO-PLA TUBB3

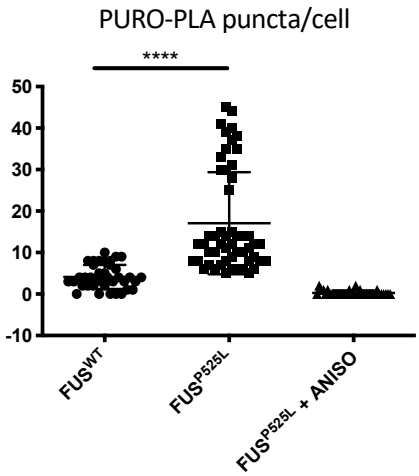

E

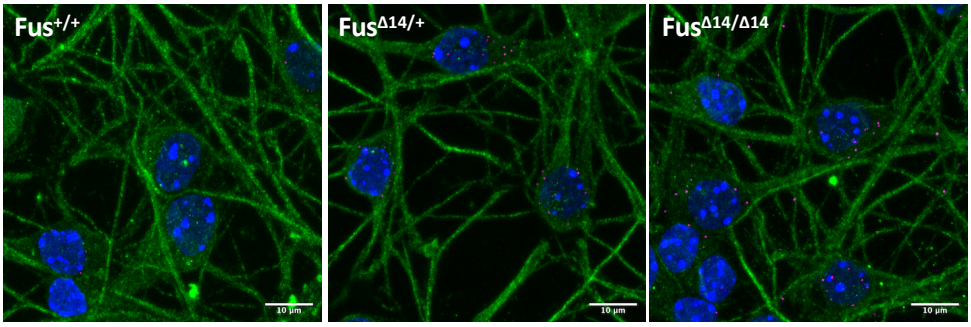

DAPI HuD PURO-PLA Tubb3

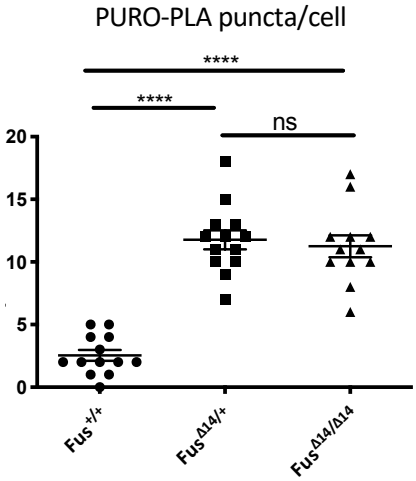

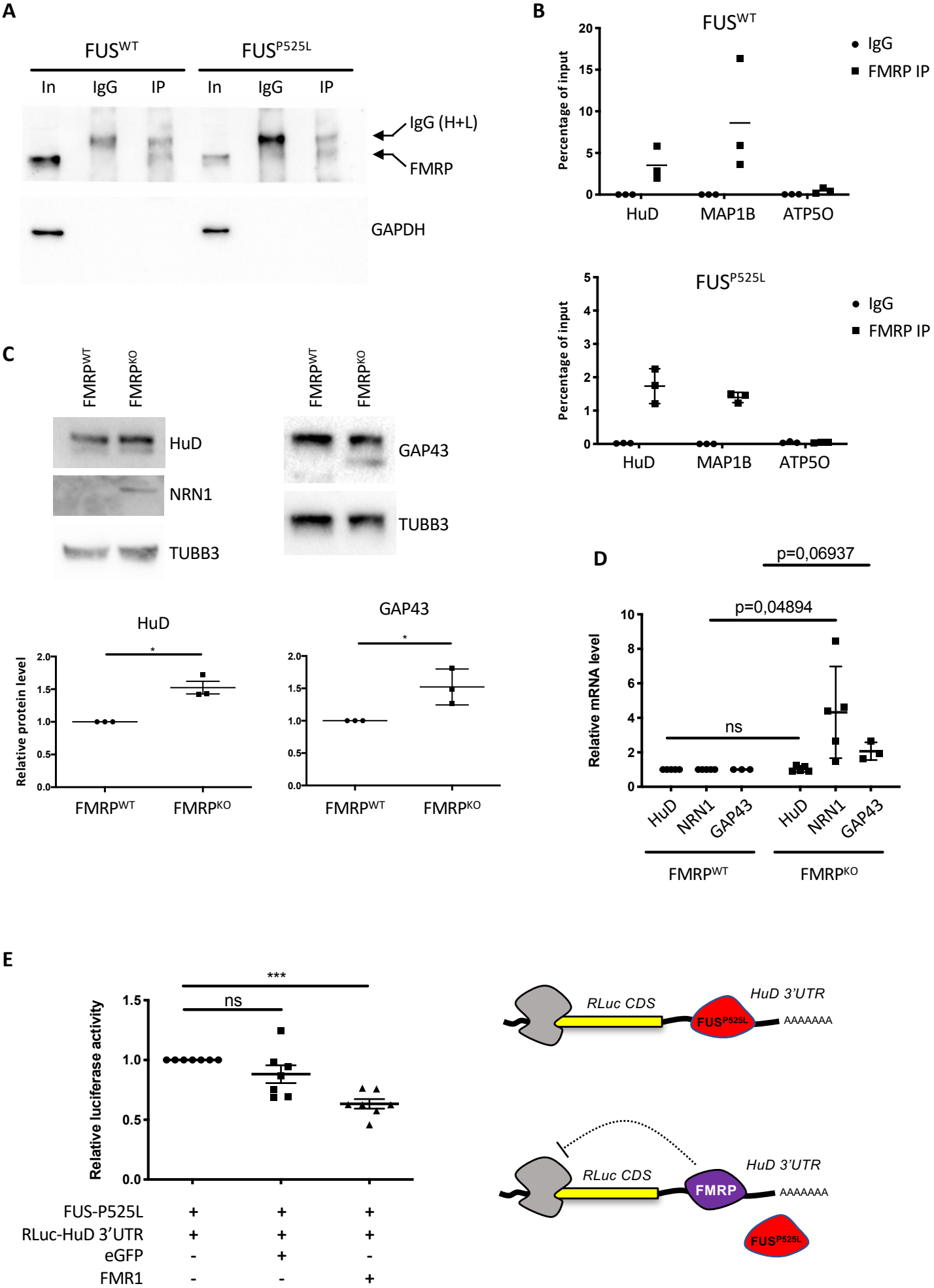
A
FUSWT
FUSP525L
In
IgG
IP
In
IgG
IP
IgG (H+L)
FMRP
GAPDH
B
FUSWT
Percentage of input
IgG
FMRP IP
HuD
MAP1B
ATP5O
FUSP525L
C
FMRPWT
FMRPKO
HuD
NRN1
TUBB3
GAP43
Relative protein level
D
p=0,06937
p=0,04894
ns
Relative mRNA level
E
Relative luciferase activity
***
ns
FUS-P525L
RLuc-HuD 3'UTR
eGFP
FMR1
RLuc CDS
HuD 3'UTR
AAAAAAA
FMRP

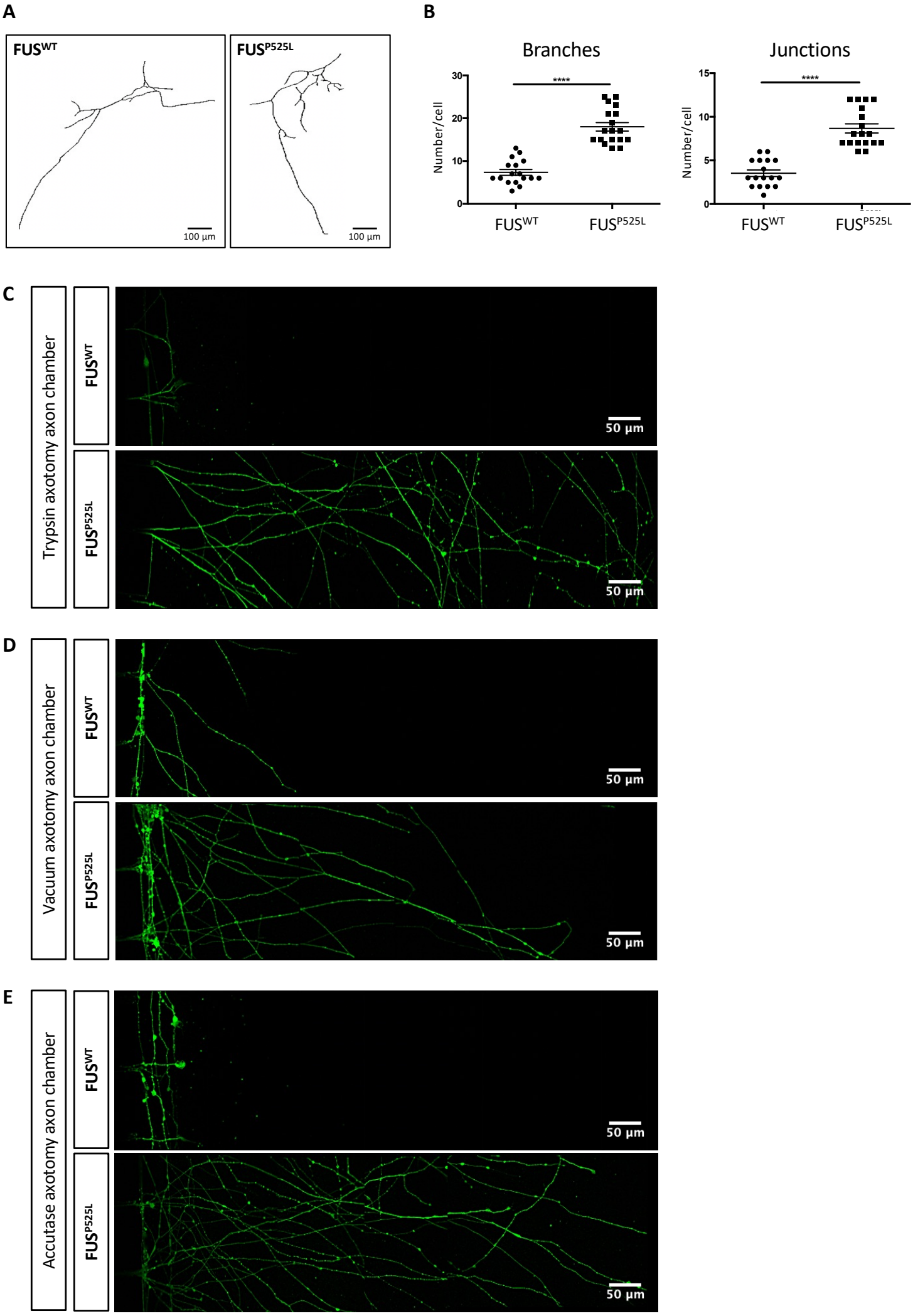
A
FUSWT
FUSP525L
100 µm
100 µm
B
Branches
Junctions
Number/cell
****
FUSWT
FUSP525L
C
Trypsin axotomy axon chamber
FUSWT
FUSP525L
50 µm
D
Vacuum axotomy axon chamber
E
Accutase axotomy axon chamber

A

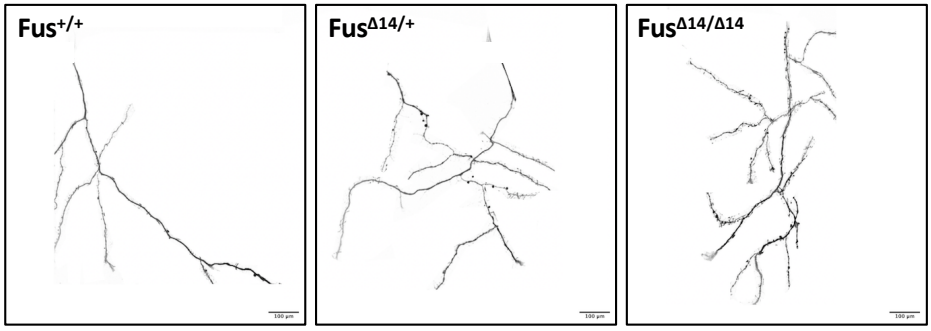
Fus+/+
FusΔ14/+
FusΔ14/Δ14

B

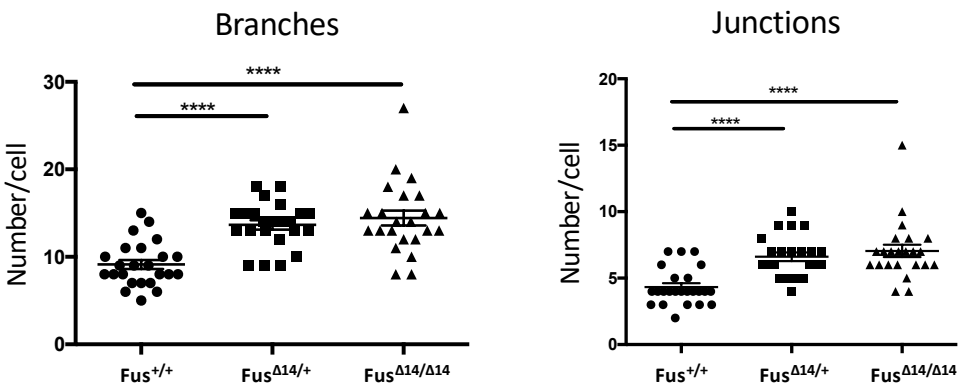
Branches
Junctions
Number/cell
****
Fus+/+
FusΔ14/+
FusΔ14/Δ14

C

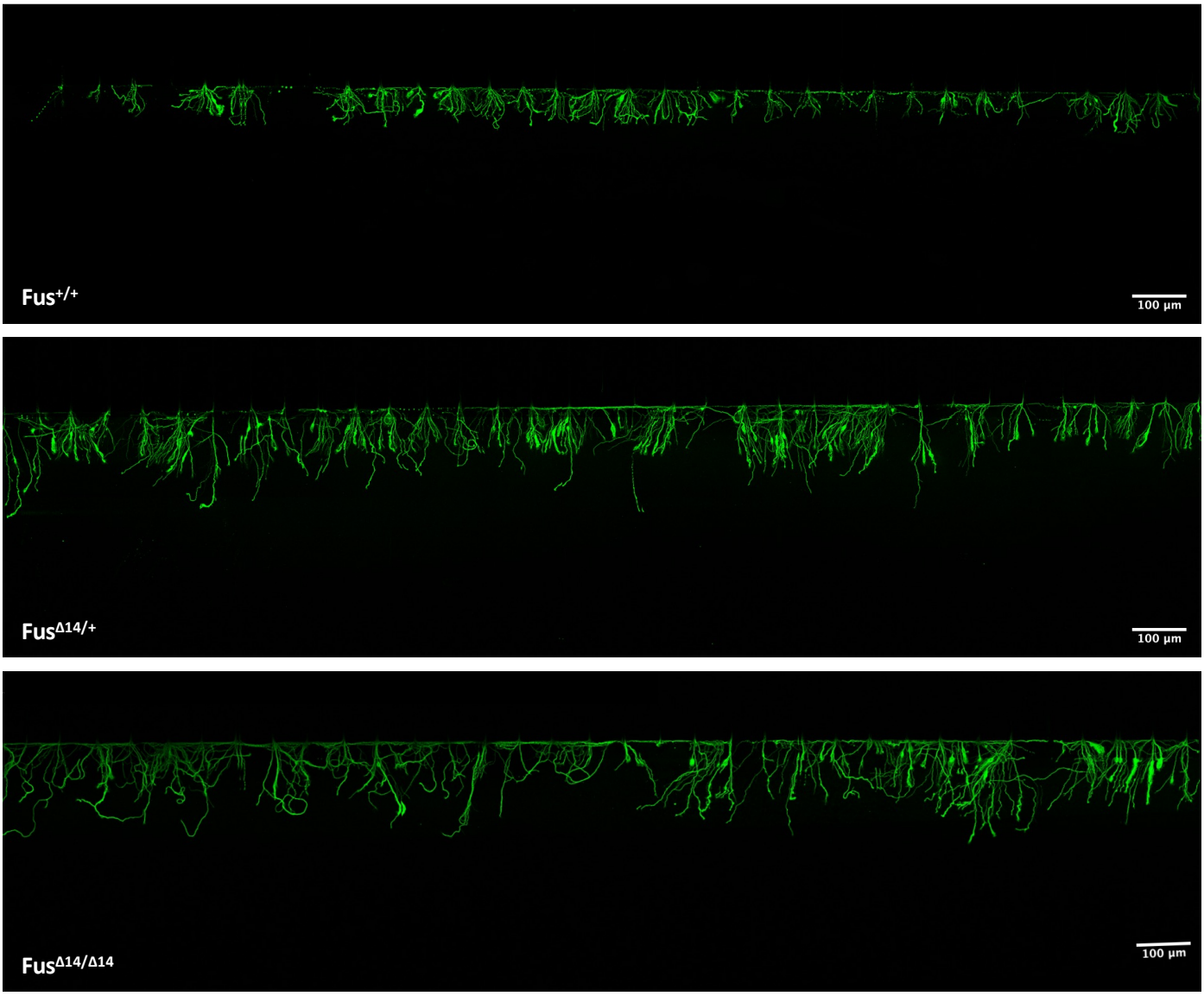
Fus+/+
FusΔ14/+
FusΔ14/Δ14
100 µm

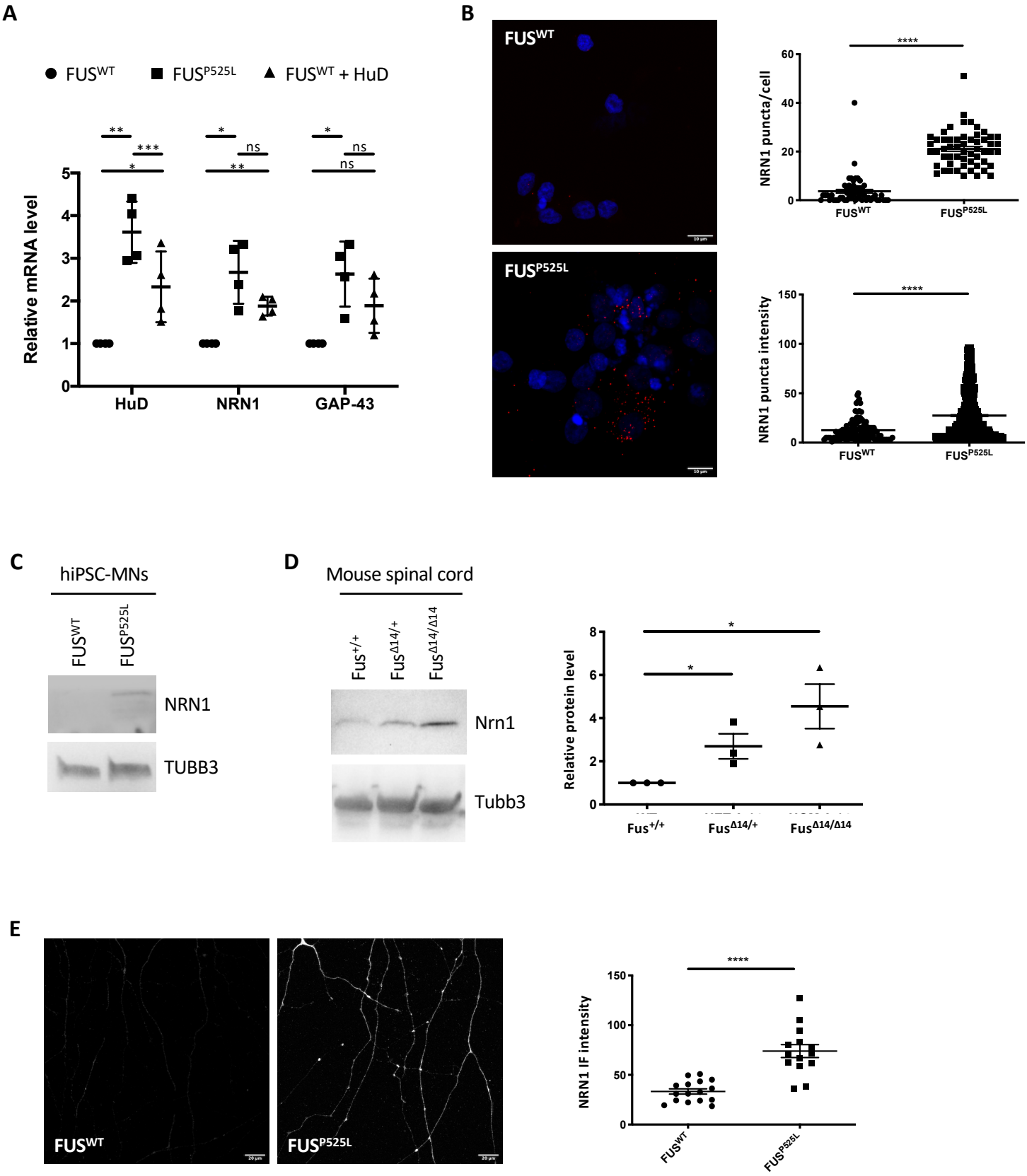
A
FUSWT
FUSP525L
FUSWT + HuD
Relative mRNA level
HuD
NRN1
GAP-43
B
FUSWT
FUSP525L
NRN1 puncta/cell
NRN1 puncta intensity
C
hiPSC-MNs
FUSWT
FUSP525L
NRN1
TUBB3
D
Mouse spinal cord
Fus+/+
FusΔ14/+
FusΔ14/Δ14
Nrn1
Tubb3
Relative protein level
E
FUSWT
FUSP525L
NRN1 IF intensity

A

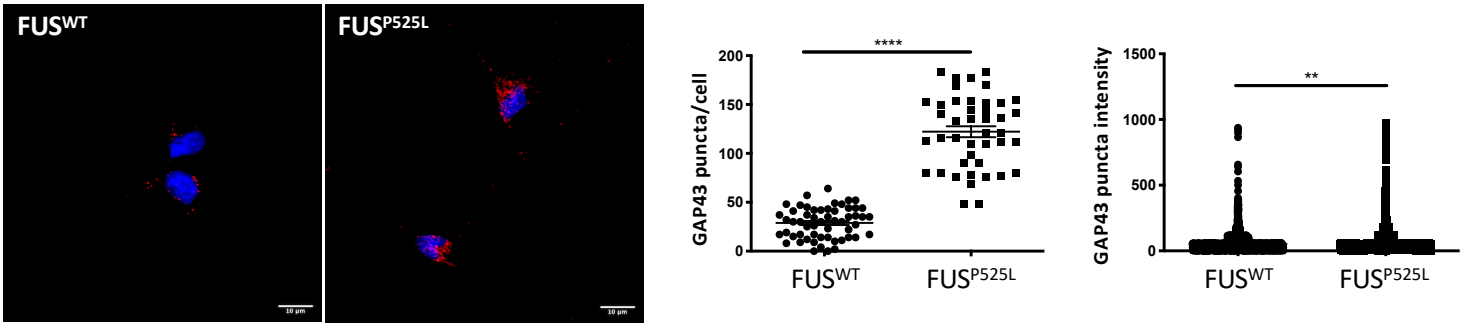
FUSWT
FUSP525L
GAP43 puncta/cell
****
FUSWT
FUSP525L
GAP43 puncta intensity
**
FUSWT
FUSP525L

B

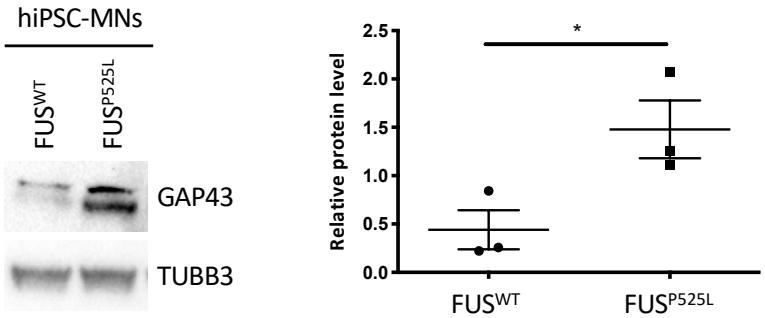
hiPSC-MNs
FUSWT
FUSP525L
GAP43
TUBB3
Relative protein level
*
FUSWT
FUSP525L

C

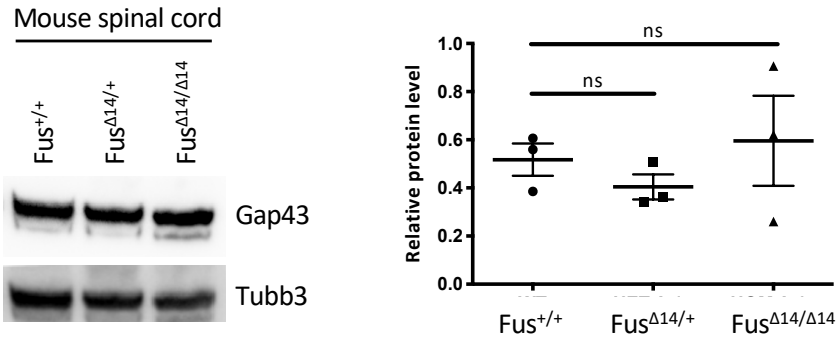
Mouse spinal cord
Fus+/+
FusΔ14/+
FusΔ14/Δ14
Gap43
Tubb3
Relative protein level
ns
ns
Fus+/+
FusΔ14/+
FusΔ14/Δ14

D

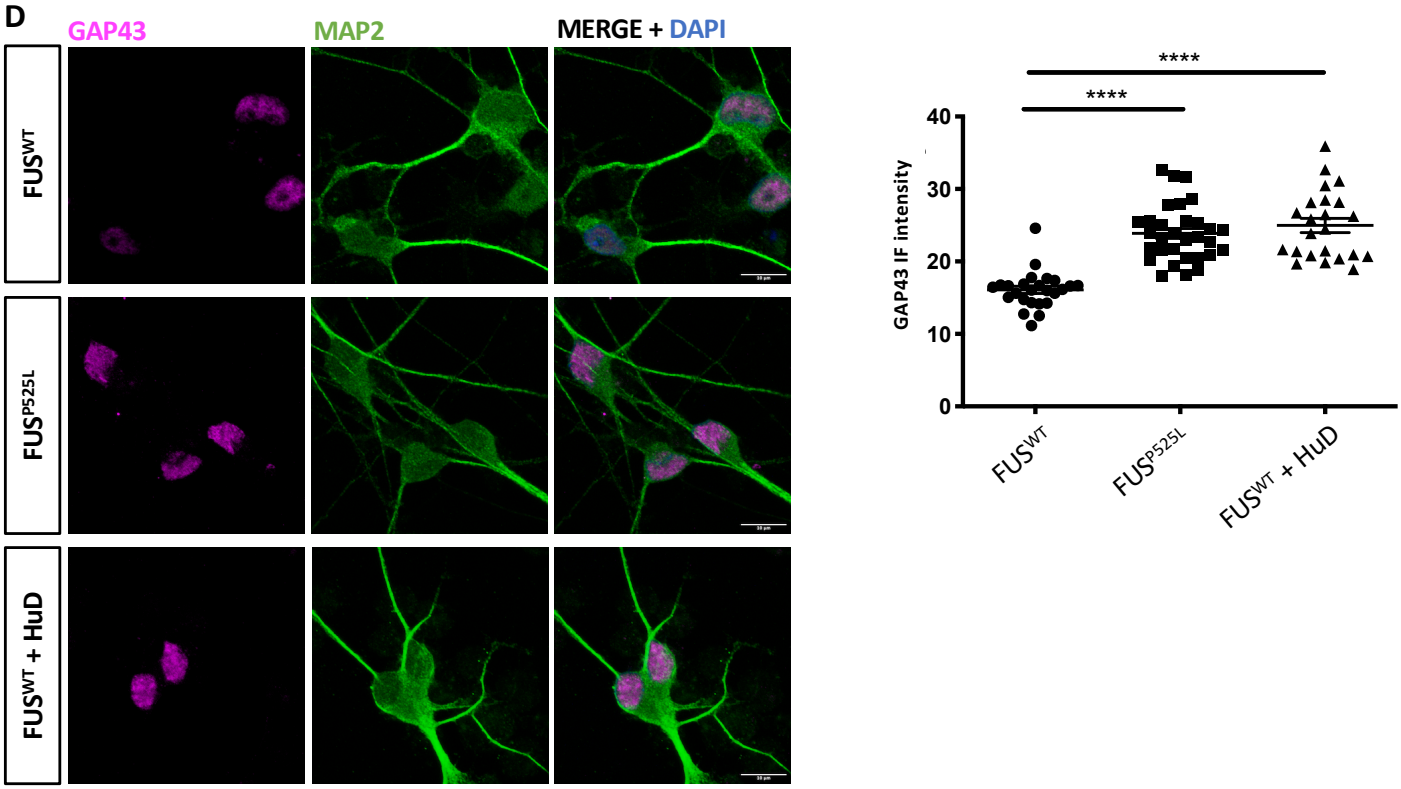
GAP43
MAP2
MERGE + DAPI
FUSWT
FUSP525L
FUSWT + HuD
GAP43 IF intensity
****
****
FUSWT
FUSP525L
FUSWT + HuD

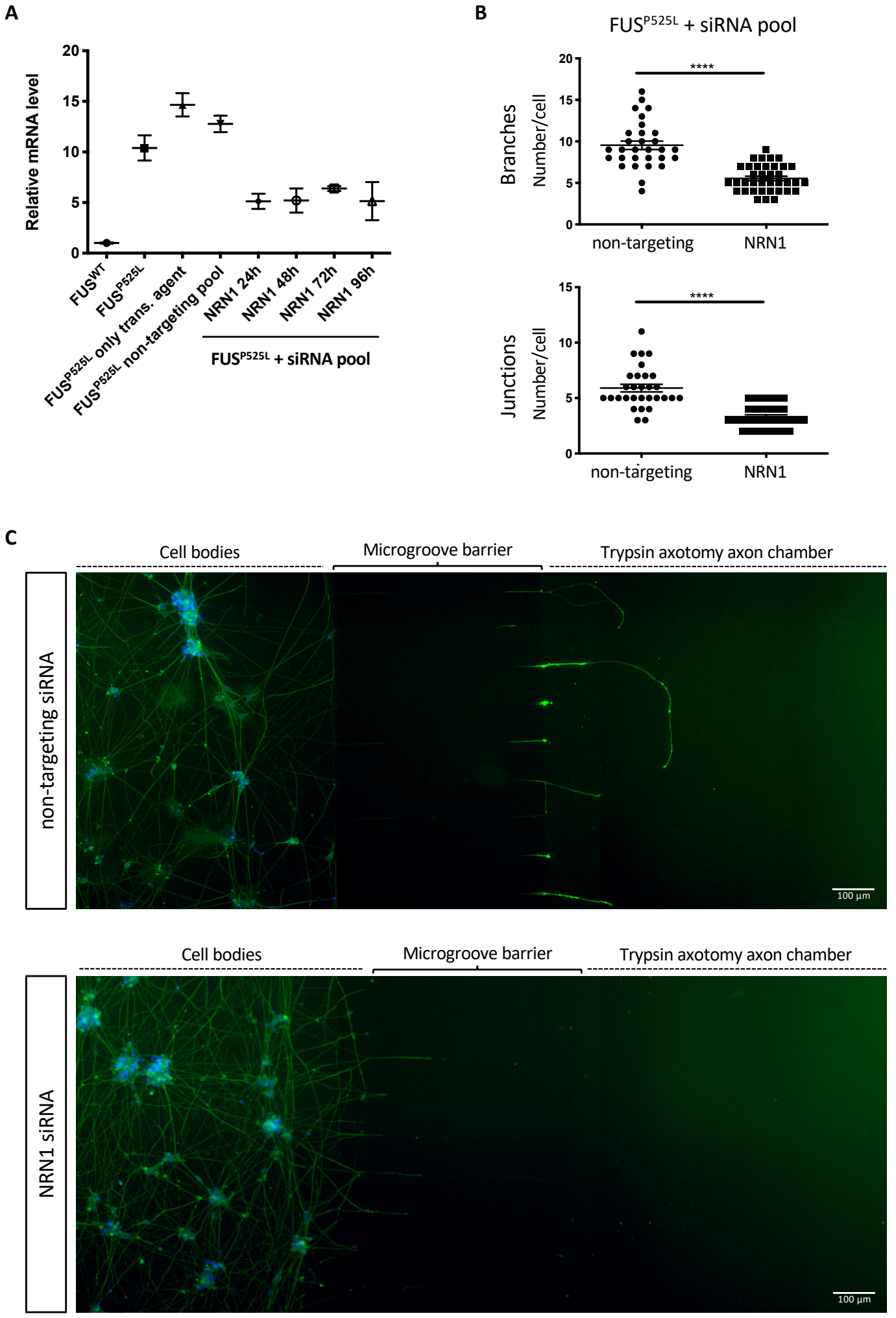
A
Relative mRNA level
20
15
10
5
0
FUSWT
FUSP525L
FUSP525L only trans. agent
FUSP525L non-targeting pool
NRN1 24h
NRN1 48h
NRN1 72h
NRN1 96h
FUSP525L + siRNA pool
B
FUSP525L + siRNA pool
Branches
Number/cell
****
non-targeting
NRN1
Junctions
Number/cell
****
non-targeting
NRN1
C
Cell bodies
Microgroove barrier
Trypsin axotomy axon chamber
non-targeting siRNA
100 µm
Cell bodies
Microgroove barrier
Trypsin axotomy axon chamber
NRN1 siRNA
100 µm

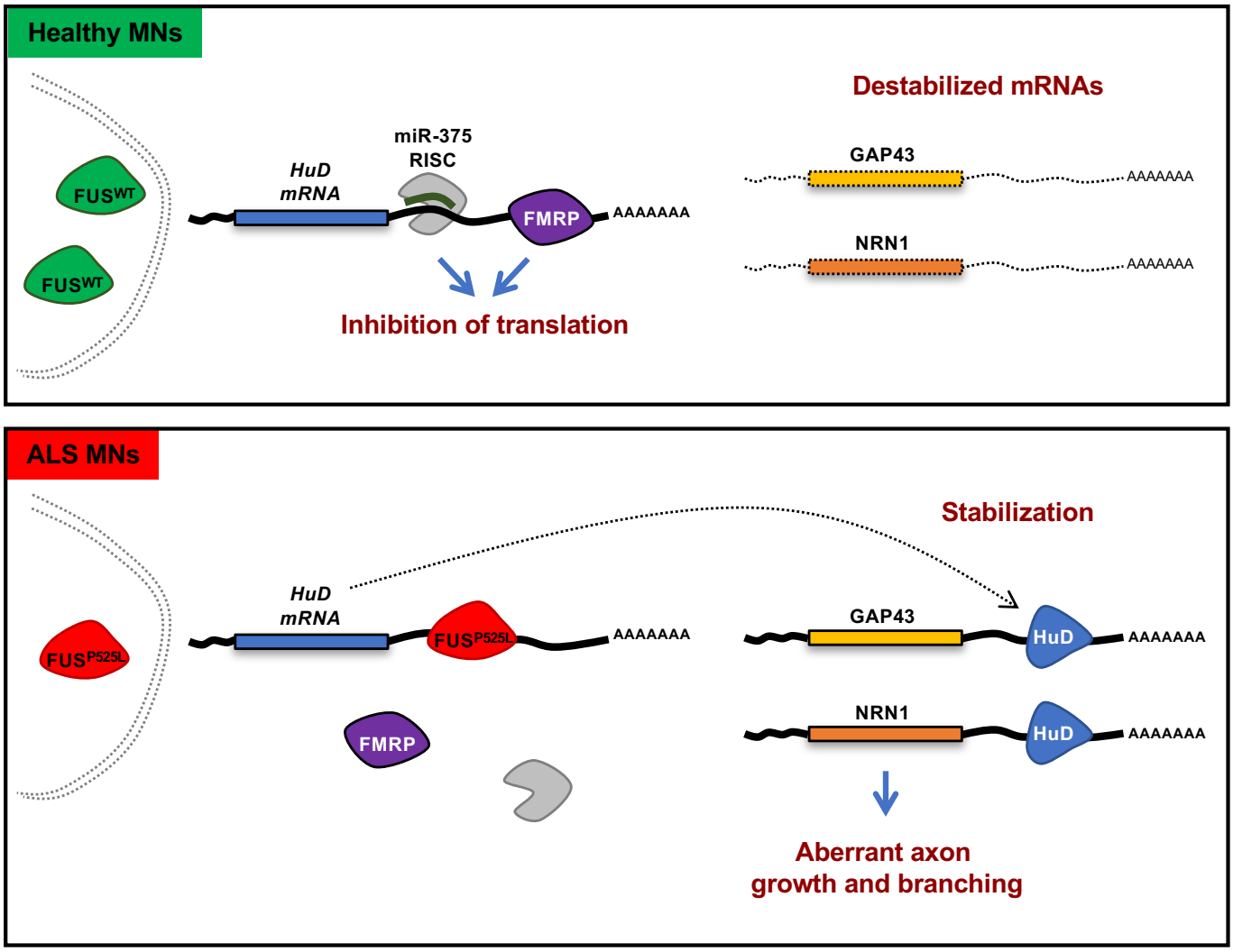
Healthy MNs
Destabilized mRNAs
miR-375
RISC
HuD
mRNA
FUSWT
FUSWT
FMRP
AAAAAAA
GAP43
AAAAAAA
NRN1
AAAAAAA
Inhibition of translation
ALS MNs
Stabilization
HuD
mRNA
FUSP525L
FUSP525L
AAAAAAA
GAP43
HuD
AAAAAAA
NRN1
HuD
AAAAAAA
FMRP
Aberrant axon
growth and branching